

Cornering Large- N_c QCD with Positivity Bounds

Clara Fernandez¹, Alex Pomarol^{1,2,3}, Francesco Riva⁴ and Francesco Sciotti¹

¹*IFAE and BIST, Universitat Autònoma de Barcelona, 08193 Bellaterra, Barcelona*

²*Departament de Física, Universitat Autònoma de Barcelona, 08193 Bellaterra, Barcelona*

³*CERN, Theory Division, Geneva, Switzerland*

⁴*Département de Physique Théorique, Université de Genève, 24 quai Ernest-Ansermet, 1211 Genève 4, Switzerland*

Abstract

The simple analytic structure of meson scattering amplitudes in the large- N_c limit, combined with positivity of the spectral density, provides precise predictions on low-energy observables. Building upon previous studies, we explore the allowed regions of chiral Lagrangian parameters and meson couplings to pions. We reveal a structure of kinks at all orders in the chiral expansion and develop analytical tools to show that kinks always correspond to amplitudes with a single light pole. We build (scalar- and vectorless) deformations of the Lovelace-Shapiro and Coon UV-complete amplitudes, and show that they lie close to the boundaries. Moreover, constraints from crossing-symmetry imply that meson couplings to pions become smaller as their spin increases, providing an explanation for the success of Vector Meson Dominance and holographic QCD. We study how these conclusions depend on assumptions about the high-energy behavior of amplitudes. Finally, we emphasize the complementarity between our results and Lattice computations in the exploration of large- N_c QCD.

1 Introduction

The understanding of theories at strong coupling is one of the most important challenges of modern particle physics. Besides the pragmatic interest for QCD hadronic physics, such understanding would broaden our perspective on theories beyond the Standard Model and plausibly provide intuition on its shortcomings.

Dispersion relations distill the essential ingredients of quantum field theory, unitarity and causality, into consistency conditions for scattering amplitudes. They have been used as *positivity bounds* to shape the parameter space of effective field theories originating from healthy, albeit strongly coupled, microscopic dynamics, see e.g. [1–7], and have had important applications to QCD and the chiral Lagrangian [8–16].

At the same time, in the context of $SU(N_c)$ gauge theories, the limit of many colors $N_c \rightarrow \infty$ has provided one of the most insightful approaches for understanding the strongly-coupled regime [17, 18], even though real-world QCD has only $N_c = 3$. The main consequence of this approximation is that the theory has a dual description in terms of weakly-coupled mesons, rather than quarks and gluons. In spite of this important step forward, the predictions of large- N_c QCD have been limited by the fact that the theory contains an infinite number of mesons of any spin, whose Lagrangian is unknown or contains an infinite number of terms.

Recently, Ref. [19] has combined these two approaches and derived important constraints on the low energy $\pi\pi \rightarrow \pi\pi$ scattering amplitude. Despite the higher-spin meson spectrum remains unknown, the simple analytic structure of large- N_c amplitudes – combined with certain assumptions on their high-energy behavior – improves the predictiveness of dispersion relations.

In this article we push forward this approach, combining analytic and numerical methods. One of the most important questions raised in Ref. [19] concerns the understanding of which theories define the kinks (and the bulk) of the allowed regions of Wilson coefficients. In this article we identify these theories. We build UV-complete four-pions amplitudes, as variations of the Lovelace-Shapiro amplitude [20, 21] and the Coon amplitude [22] in which the spin-0 (and spin-1) poles have been removed, and show that they reside close to the boundary. At the kinks, on the other hand, we find theories with an infinitely degenerate higher-spin spectrum, or theories with a unique state at finite mass, either of spin $J = 0$, $J = 1$ or $J = 2$. While some of these results are known [4, 6, 19], in this work we are able to exclude other possibilities. In particular, while the numerical approach suggests the existence of a new kink with a more exotic spectrum, we show that the kink position can be reformulated as a 1D moment-problem whose solution converges to the $J = 1$ theory.

An important emerging property of low-energy QCD is Vector Meson Dominance (VMD) [23], the hypothesis that the spin-1 ρ meson gives the main contribution to the chiral Lagrangian [24]. This property has an empirical origin (it works!), but it lacks a theoretical explanation. We will show that VMD finds its origin in the positivity bounds. Indeed, the chiral Lagrangian coefficients can be written as a sum over positive quantities that depend on the couplings and masses of the different mesons: when the theory contains a ρ , this dominates over the other $J > 1$ states. This is especially prominent when the higher-spin states are heavier than the ρ , as it occurs in real-world QCD. Our analysis also provides insight into why holographic models, which contain only (charged) spin-0 and spin-1 states, have been so successful in predicting

low-energy properties of QCD, see e.g. [25, 26]. Finally, we will show that this reasoning also extends to the heavy-meson couplings to pions: the higher the spin, the smaller the coupling.

These arguments, as well as all those from Ref. [19], rely on assuming that the high-energy amplitudes are particularly well behaved, $\mathcal{M}/s \rightarrow 0$ at large $|s|$. In this article we will also discuss the implications of relaxing this assumption, such that the $\pi\pi \rightarrow \pi\pi$ amplitude is limited only by the Froissart-Martin bound $\mathcal{M}/s^2 \rightarrow 0$ at large energies [27, 28]. In this case, the spin-1 and spin-0 contributions decouple from (and can contribute more than) the $J \geq 2$ ones, that are now dominated by the spin-2 state instead, in a generalisation of VMD.

The paper is organised as follows. In Sec. 2 we review the analytical structure of the $\pi\pi \rightarrow \pi\pi$ amplitude and the dispersion relations that lead to positivity constraints. We also present possible UV completions to the chiral Lagrangian, as they will play an important role to understand the boundaries of the Wilson-coefficient allowed regions. In Sec. 3 we consider the case in which the four-pion amplitude at large $|s|$ satisfies $\mathcal{M}/s \rightarrow 0$. We determine the allowed regions of the leading Wilson coefficients and show which theories reside at the kinks of these boundaries. We also study the emergence of VMD and derive bounds on the couplings of meson resonances to pions. In Sec. 4 we extend the analysis to the case in which the four-pion amplitude only satisfies the Froissart-Martin bound at high energies. We present several appendices with extended discussions on the numerical bootstrap (Appendix A), on the analytical determination of the kinks (Appendix B), the su -models (Appendix C), and the Lovelace-Shapiro and Coon amplitudes (Appendix D and Appendix E respectively).

2 The $\pi\pi \rightarrow \pi\pi$ Amplitude in large- N_c QCD

This section contains mostly a review of previous literature on the $2 \rightarrow 2$ pion amplitude, in particular the results of Ref. [19]. We will work in the massless quark limit.

Pions are the massless Goldstone bosons associated to the spontaneous breaking of the global $SU(N_f)_L \times SU(N_f)_R \rightarrow SU(N_f)$, where N_f is the number of quark flavors in QCD. They transform in the *Adj.* representation of $SU(N_f)$, which for the case $N_f = 2$ corresponds to the Isospin $I = 1$, the triplet π^\pm and π^0 . This allows us to write the $2 \rightarrow 2$ pion amplitude as

$$\mathcal{M}(\pi^a \pi^b \rightarrow \pi^c \pi^d) = A(s|t, u) \left[\frac{2}{N_f} \delta_s + d_s \right] + A(t|u, s) \left[\frac{2}{N_f} \delta_t + d_t \right] + A(u|s, t) \left[\frac{2}{N_f} \delta_u + d_u \right], \quad (1)$$

where $s = (p_a + p_b)^2$, $t = (p_a - p_c)^2$, $u = (p_a - p_d)^2$, and

$$\delta_s = \delta_{ab} \delta_{cd}, \quad \delta_t = \delta_s(b \leftrightarrow c), \quad \delta_u = \delta_s(b \leftrightarrow d), \quad (2)$$

$$d_s = d_{abe} d_{cde}, \quad d_t = d_s(b \leftrightarrow c), \quad d_u = d_s(b \leftrightarrow d), \quad (3)$$

correspond to the various ways of contracting $SU(N_f)$ adjoint indices into singlets. $A(s|t, u)$ is a function of t, u symmetric under their interchange, i.e. $A(s|t, u) = A(s|u, t)$.

In the large- N_c limit, QCD reduces to a theory of weakly coupled mesons, whose trilinear couplings scale as $\sim 1/\sqrt{N_c}$ [17, 18]. In this limit, the $2 \rightarrow 2$ pion amplitude is then dominated

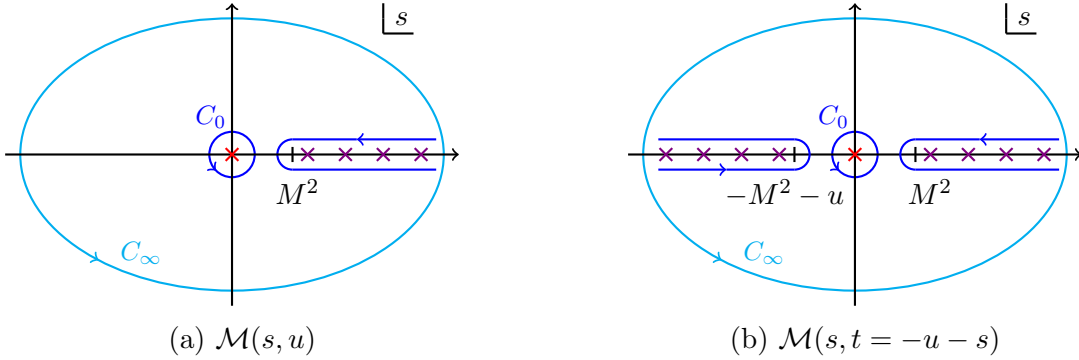


Figure 1: Analytic structure of $\mathcal{M}(s, u)$ and $\mathcal{M}(s, t = -s - u)$ for fixed $u < 0$. We denote by C_0, C_∞ (to be taken at $|s| \rightarrow \infty$) and the discontinuity along the real axis the relevant contours of integration used for dispersion relations.

by a tree-level meson exchange. Since these mesons are $q\bar{q}$ states with isospin $I = 0, 1$, the isospin $I = 2$ amplitude,

$$\mathcal{M}_s^{I=2}(\pi^a \pi^b \rightarrow \pi^c \pi^d) = A(t|u, s) + A(u|s, t) \equiv \mathcal{M}(t, u), \quad (4)$$

(symmetric under $t \leftrightarrow u$) has no poles in the large- N_c limit. All this leads to the following important implications for the analytical structure of \mathcal{M} in the large- N_c limit:

- The only singularities of \mathcal{M} in the complex s -plane are simple poles associated with the tree-level meson exchange (the branch cut along the physical region is at least $O(1/N_c^2)$).
- The absence of $I = 2$ meson exchange in the s -channel implies that $\mathcal{M}_s^{I=2} = \mathcal{M}(t, u)$ has no poles for real $s > 0$. Since $t = -s - u$, this implies that for fixed $u < 0$, there cannot be poles in $\mathcal{M}(t, u)$ on the negative real t axis. Now, by a simple exchange of arguments ($t \rightarrow s$), we come to the conclusion that $\mathcal{M}(s, u)$, for fixed $u < 0$, can only have poles on the positive real s axis.
- For fixed $u < 0$, $\mathcal{M}(s, t)$ can have poles either on the real positive or negative s axis.

This analytic structure of \mathcal{M} is illustrated in Fig. 1.

At energies below the mass M of the lightest massive meson (corresponding to the position of the first pole in Fig. 1), pions can be well described by an effective theory, corresponding to an expansion in $s/M, u/M \rightarrow 0$,

$$\begin{aligned} \mathcal{M}(s, u) &= \sum_{n=1}^{\infty} \sum_{l=0}^{[n/2]} g_{n,l} s^{\{n-l\}} u^l \\ &= g_{1,0}(s+u) + g_{2,0}(s^2+u^2) + g_{2,1}su + g_{3,0}(s^3+u^3) \\ &+ g_{3,1}(s^2u+su^2) + g_{4,0}(s^4+u^4) + g_{4,1}(s^3u+su^3) + g_{4,2}s^2u^2 + \dots, \end{aligned} \quad (5)$$

where for convenience we have defined the weighed symmetric tensor $s^{\{i\}}u^j \equiv s^i u^j + (1 - \delta_{ij})s^j u^i$ to avoid double counting of terms with $n = 2l$, such as $g_{2,1}, g_{4,2}$, etc. A constant term is absent

in Eq. (5) as the amplitude must go to zero for $s, u \rightarrow 0$ in order to restore the Adler condition for pions. In the large- N_c limit all Wilson coefficients scale as $g_{n,l} \sim 1/N_c$. For the connection of Eq. (5) with the QCD chiral Lagrangian, see Sec. 3.2.1.

2.1 Dispersion Relations and Sum Rules

Dispersion relations can be derived assuming that the amplitude \mathcal{M} satisfies the following high-energy conditions, for fixed $u < 0$ and for all $k \geq k_{\min}$,

$$\lim_{|s| \rightarrow \infty} \frac{\mathcal{M}(s, u)}{s^k} \rightarrow 0, \quad (6a) \quad \lim_{|s| \rightarrow \infty} \frac{\mathcal{M}(s, -u - s)}{s^k} \rightarrow 0. \quad (6b)$$

Different assumptions about the high-energy behavior of amplitudes are associated with different values of k_{\min} . On general grounds, the Froissart-Martin bound [27–29] ensures that in theories with a mass gap Eqs. (6) are satisfied for $k_{\min} = 2$, with similar results for the massless case [7, 30, 31].

On the other hand, Ref. [19] advocated – invoking considerations on the Pomeron Regge trajectory – that the four-pion amplitude might be bounded by $\mathcal{M} \lesssim s$ and therefore $k_{\min} = 1$. In this article we will study both, the case with $k_{\min} = 1$ and $k_{\min} = 2$.

2.1.1 IR-UV Relations

Taking $u < 0$ fixed, we have that the integral of $\mathcal{M}(s, u)/s^{k+1}$ along the contour C_∞ of Fig. 1a vanishes for $k \geq k_{\min}$, due to Eq. (6a). Because of amplitude’s analyticity, we can deform C_∞ into the blue contour in Fig. 1a,

$$\oint_{C_0} ds' \frac{\mathcal{M}(s', u)}{s'^{k+1}} = 2i \int_{M^2}^{\infty} ds' \frac{\text{Im}\mathcal{M}(s', u)}{s'^{k+1}}. \quad (7)$$

The amplitude can be expanded in partial waves,

$$\text{Im}\mathcal{M}(s, u) = \sum_J (2J + 1) \rho_J(s) P_J \left(1 + \frac{2u}{s} \right), \quad (8)$$

where P_J are the Legendre polynomials and $\rho_J(s)$, the spectral density, must be positive, $\rho_J(s) \geq 0$, due to unitarity of the S-Matrix. Indeed, for large- N_c theories, we have that the spectral density is given by

$$(2J + 1) \rho_J(m^2) = \pi \sum_i g_{i\pi\pi}^2 m_i^2 \delta(m^2 - m_i^2) \delta_{JJ_i}, \quad (9)$$

where i labels mesons of mass m_i , spin J_i and coupling to pions $g_{i\pi\pi}$.

Plugging Eq. (8) into Eq. (7), performing the contour integrals, and expanding around small $u < 0$ we find

$$\begin{aligned}
k = 1 : \quad g_{1,0} + g_{2,1}u + g_{3,1}u^2 + \dots &= \left\langle \frac{P_J(1)}{m^2} + 2\frac{P'_J(1)}{m^4}u + 2\frac{P''_J(1)}{m^6}u^2 + \dots \right\rangle, \\
k = 2 : \quad g_{2,0} + g_{3,1}u + g_{4,2}u^2 + \dots &= \left\langle \frac{P_J(1)}{m^4} + 2\frac{P'_J(1)}{m^6}u + 2\frac{P''_J(1)}{m^8}u^2 + \dots \right\rangle, \\
k = 3 : \quad g_{3,0} + g_{4,1}u + g_{5,2}u^2 + \dots &= \left\langle \frac{P_J(1)}{m^6} + 2\frac{P'_J(1)}{m^8}u + 2\frac{P''_J(1)}{m^{10}}u^2 + \dots \right\rangle, \\
&\vdots
\end{aligned} \tag{10}$$

with the definition of the high-energy average [6],

$$\langle (\dots) \rangle \equiv \frac{1}{\pi} \sum_J (2J+1) \int_{M^2}^{\infty} \frac{dm^2}{m^2} \rho_J(m^2) (\dots). \tag{11}$$

Considering equations with $k \geq k_{\min}$ (that we will take later to be $k_{\min} = 1, 2$), we can relate the IR Wilson coefficients with the UV-averages of derivatives of P_J in the following way:

$$g_{n+l,l} = \frac{2^l}{l!} \left\langle \frac{P_J^{(l)}(1)}{m^{2(n+l)}} \right\rangle, \quad n \geq k_{\min} \text{ and } l = 0, 1, \dots, \left[\frac{n-1}{2} \right]. \tag{12}$$

Since $P_J^{(l)}(1) \geq 0$, the contributions to Eq. (12) from the different J -states are always additive, and therefore $g_{n+l,l} \geq 0$ – this is a direct consequence of the lack of $s < 0$ poles in $\mathcal{M}(s, u)$. Moreover, $P_J^{(l)}(1) = 0$ for $l > J$ implying that states with $J \leq l$ do not contribute to $g_{n+l,l}$.

In particular,

$$\begin{aligned}
g_{n,0} &= \left\langle \frac{1}{m^{2n}} \right\rangle = \sum_i \frac{g_{i\pi\pi}^2}{m_i^{2n}}, \\
g_{n+1,1} &= \left\langle \frac{\mathcal{J}^2}{m^{2(n+1)}} \right\rangle = \sum_i \frac{g_{i\pi\pi}^2 J_i(J_i+1)}{m_i^{2(n+1)}}, \\
g_{n+2,2} &= \frac{1}{4} \left\langle \frac{\mathcal{J}^4 - 2\mathcal{J}^2}{m^{2(n+1)}} \right\rangle = \sum_i \frac{g_{i\pi\pi}^2 J_i(J_i-1)(J_i+1)(J_i+2)}{4m_i^{2(n+1)}},
\end{aligned} \tag{13}$$

where $\mathcal{J}^2 \equiv J(J+1)$. Notice that only for $k_{\min} = 1$ all Wilson coefficients have a dispersive representation in terms of Eq. (12). For $k_{\min} = 2$, the couplings $g_{1,0}$ and $g_{2,1}$ are not captured by these dispersion relations.

In a similar way, we can obtain dispersion relations for the $\mathcal{M}(s, t)$ amplitude, whose analytic structure is given in Fig. 1b,

$$\frac{1}{2i} \oint_{C_0} ds' \frac{\mathcal{M}(s', -u - s')}{s'^{k+1}} = \int_{M^2}^{\infty} ds' \frac{\text{Im}\mathcal{M}(s', -u - s')}{s'^{k+1}} + (-1)^k \int_{M^2}^{\infty} ds' \frac{\text{Im}\mathcal{M}(s', -u - s')}{(s' + u)^{k+1}}. \tag{14}$$

These can be expanded as in the previous section, and provide yet more relations [19]. In the case $k_{\min} > 1$ these new relations are crucial, as they give access to Wilson coefficients that do not have a dispersive representation in terms of $\mathcal{M}(s, u)$. In particular, for $k_{\min} = 2$, the coupling $g_{2,1}$ is not determined by Eq. (12) but appears in Eq. (14),

$$g_{2,1} = 2g_{2,0} - 2 \left\langle \frac{(-1)^J}{m^4} \right\rangle, \quad (15)$$

while for $k_{\min} = 3$, $g_{3,1}$ can only be determined by

$$g_{3,1} = 3g_{3,0} + \left\langle \frac{(-1)^J(2\mathcal{J}^2 - 3)}{m^6} \right\rangle. \quad (16)$$

2.2 Null Constraints

The dispersion relations in Eq. (10), and the small- u expansion of Eq. (14), over-determine the Wilson coefficients. This leads to a set of *null constraints*,

$$\langle \mathcal{X}_{n,k}(J, m^2) \rangle = 0, \quad \langle \mathcal{Y}_{n,k}(J, m^2) \rangle = 0, \quad (17)$$

on the high-energy spectral density, with $m^{2n}\mathcal{X}_{n,k}$ and $m^{2n}\mathcal{Y}_{n,k}$ functions of J only. Their compact expression at all orders is provided in Ref. [19]. For the analytic arguments in this article we are only interested in the most relevant null constraints (those involving less powers of $1/m$) and in those with the leading asymptotic $J \rightarrow \infty$ behavior at a fixed order n in $1/m^{2n}$.

For $k_{\min} = 1$, there is one (and only one) null constraint $\sim O(J^{2(n-1)}/m^{2n})$ at each order n ,¹

$$\begin{aligned} n = 2 : \quad m^4 \mathcal{Y}_{2,1} &= -2(1 - (-1)^J) + \mathcal{J}^2, \\ n = 3 : \quad m^6 \mathcal{X}_{3,1} &= -6\mathcal{J}^2 + \mathcal{J}^4, \\ n = 4 : \quad m^8 \mathcal{X}_{4,1} &= -24\mathcal{J}^2 - 8\mathcal{J}^4 + \mathcal{J}^6, \\ &\vdots \\ (n-1)!^2 m^{2n} \mathcal{X}_{n,1} &= \frac{2^{n-1}}{(n-1)!} P_J^{(n-1)}(1) - \mathcal{J}^2. \end{aligned} \quad (18)$$

The other null constraints have only subleading terms in powers of J w.r.t. these.

When we study larger k_{\min} , the constraints in Eq. (18) disappear, and subleading null constraints now dominate. For $k_{\min} = 2$ this involves null constraints that grow as $O(J^{2(n-2)}/m^{2n})$. There are two of them at each order n , and can be separated into those where the sign of the term $O(J^{2(n-2)}/m^{2n})$ is fixed, and those where this sign oscillates between J -odd and J -even.

¹We use a slightly different normalization w.r.t. Ref. [19], which has no impact on Eq. (17).

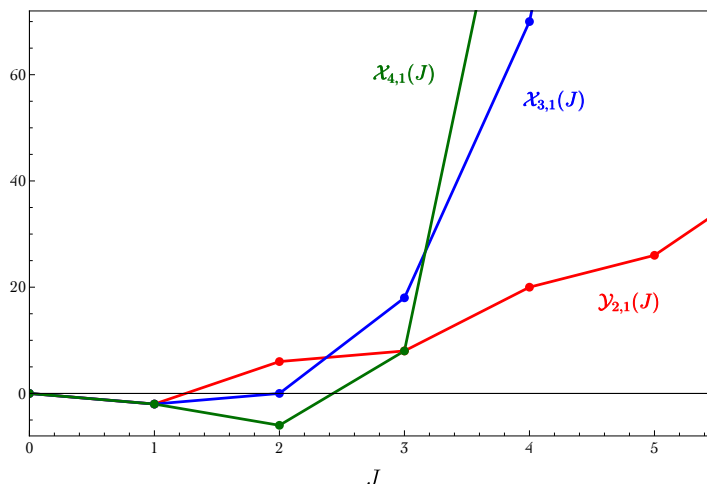


Figure 2: Null constraints from Eq. (18), as a function of J , for fixed m .

In the first class we have,

$$\begin{aligned}
n = 4 : \quad m^8 (\mathcal{Y}_{4,2} - \mathcal{Y}_{4,1}) &= 8(1 - (-1)^J) - 10\mathcal{J}^2 + \mathcal{J}^4, \\
n = 5 : \quad m^{10} \mathcal{X}_{5,2} &= 30\mathcal{J}^2 - 17\mathcal{J}^4 + \mathcal{J}^6, \\
n = 6 : \quad m^{12} \mathcal{X}_{6,2} &= 144\mathcal{J}^2 - 46\mathcal{J}^4 - 20\mathcal{J}^6 + \mathcal{J}^8, \\
&\vdots \\
(n-2)!^2 m^{2n} \mathcal{X}_{n,2} &= \frac{2^{n-2}}{(n-2)!} P_J^{(n-2)}(1) - 2P_J^{(2)}(1). \tag{19}
\end{aligned}$$

In both cases, Eq. (18) and Eq. (19), the $\mathcal{Y}_{n,k}$ null constraints (originating from $\mathcal{M}(s, t)$ dispersion relations) appear only at the lowest order in $1/m^2$, and at higher order the dominant J behavior is controlled by the $\mathcal{X}_{n,k}$ null constraints (originating from $\mathcal{M}(s, u)$ dispersion relations). On the other hand, the most relevant oscillating null constraint is,

$$n = 3 : \quad m^6 \mathcal{Y}_{3,1} = -6(1 - (-1)^J) + 2(1 - 2(-1)^J)\mathcal{J}^2, \tag{20}$$

where the sign of the \mathcal{J}^2 term oscillates with J .

Notice that for $J = 0$ the arguments of all null constraints vanish, as can be easily seen in Eq. (18) and Eq. (19) (and more generally by the expressions in Ref. [19]). This implies that the spin-0 component of the UV spectrum decouples and is not restricted by null constraints. This is related to the fact that models with only $J = 0$ states can provide a consistent UV completion of the pion amplitude, satisfying Eq. (6a) and Eq. (6b) for $k_{\min} = 1$, as we will discuss in section 2.3. For $k_{\min} = 2$, also $J = 1$ states give zero contributions and decouple from the null constraints. This again can be understood from the fact that models with only $J = 1$ states provide a pion amplitude that consistently satisfies the Froissart-Martin bound. This pattern persists: for $k_{\min} = 3$, one finds that the $J = 0, 1, 2$ states decouple from the null constraints, and so on.

It is also instructive to understand how the null constraints can be satisfied, as this tells us information about the mass spectrum of the theories. In Fig. 2 we show the first few null constraints in Eq. (18) as a function of J . We see that for the first two null constraints the contribution from the $J = 1$ is the only opposite in sign to the other ones. As these expressions must average to zero, Eq. (11), this implies that the theory must contain $J = 1$ states. For $\mathcal{X}_{4,1}$, also the $J = 2$ contribution is negative, implying that also $J = 2$ states are needed. As the order n of the null constraint increases, one finds that the number of states with negative coefficients increases: eventually all J are needed to satisfy the null constraints. So, for $k_{\min} = 1$, theories in the large- N_c limit either have no $J > 0$ state, or have states with all values of J from 1 to ∞ . Similarly, for $k_{\min} = 2$, states with spin $J \geq 2$ are either absent, or are all present.

2.3 UV completions of the pion amplitude

Before proceeding to examine the implications from positivity, we would like to discuss simple UV completions for a theory of pions. By this we mean theories that generate consistent crossing-symmetric amplitudes $\mathcal{M}(s, u)$, with simple poles at real $s > 0$, positive spectral density, satisfying the high-energy behavior of Eqs. (6) for some k_{\min} . Interestingly, these amplitudes will turn out to reside at the kinks of the allowed parameter space, as we will discuss in the next section.

Simple amplitudes describing exchange of a single spin- J particle with mass m_J are characterised by a pole-structure with residue on the associated partial wave,

$$\mathcal{M}^J(s, u) = \frac{m_J^2 P_J(1 + 2u/m_J^2)}{m_J^2 - s} + F(s, u) + (s \leftrightarrow u), \quad (21)$$

where F is an analytic function that defines the theory, but does not contribute to the residue. We will fix F by imposing the Adler's zero $\mathcal{M}^J(0, 0) = 0$ and by requiring that the amplitude satisfies the large- s behavior of Eqs. (6) for the lowest possible value of k_{\min} .

2.3.1 Theory of scalars

Scalars can provide a consistent UV completion to a theory of pions, via the Higgs mechanism in the linear sigma-model. The $2 \rightarrow 2$ pion amplitude mediated by a spin-0 state with $I = 0$ is given by,

$$\mathcal{M}^{(s)}(s, u) = \frac{g_{s\pi\pi}^2 s}{m_s^2 - s} + (s \leftrightarrow u). \quad (22)$$

Expanding Eq. (22) at low energies, $s, u \ll m_s^2$, we obtain,

$$g_{n,0} = \frac{g_{s\pi\pi}^2}{m_s^{2n}} \quad (n \geq 1), \quad g_{n,l} = 0 \quad (l \neq 0). \quad (23)$$

An important property of Eq. (22) is that it satisfies the high-energy behavior in Eqs. (6a,6b) with $k_{\min} = 1$. Therefore the Wilson coefficients Eq. (23) obey the sum rules Eq. (13), as can be easily checked. The fact that a model of only scalars does not need higher-spin states to satisfy Eqs. (6a,6b) with $k_{\min} = 1$, explains why the $J = 0$ states decouple from the null constraints, as explained above.

2.3.2 Theory of vectors

Let us now consider a (weakly coupled) spin-1 resonance with isospin $I = 1$ (or, in general, in the *Adj.* representation of $SU(N_f)$), which we will refer to as ρ , in analogy with QCD. From Eq. (21) we have,

$$\mathcal{M}^{(\rho)}(s, u) = \frac{g_{\rho\pi\pi}^2 m_\rho^2}{m_\rho^2 - s} P_1 \left(1 + \frac{2u}{m_\rho^2} \right) + (s \leftrightarrow u), \quad (24)$$

corresponding to the contribution from the transverse components of a massive vector coupling to pions via $g_{\rho\pi\pi} f_{abc} \rho_\mu^a \pi^b \partial^\mu \pi^c$ (minimal coupling) where f_{abc} are the $SU(N_f)$ structure constants.² This amplitude can arise in models in which the ρ gets its mass from the Higgs mechanism, or in holographic models where the ρ arises as a Kaluza-Klein state.

Eq. (24) satisfies the Froissart-Martin bound, Eqs. (6a,6b) but only for $k_{\min} = 2$. Nevertheless, the high-energy behaviour of Eq. (24) can be improved by the following deformation [19]:

$$\widehat{\mathcal{M}}^{(\rho)}(s, u) = \frac{g_{\rho\pi\pi}^2 m_\rho^2}{m_\rho^2 - s} P_1 \left(1 + \frac{2u}{m_\rho^2} \right) \frac{m_\infty^2}{m_\infty^2 - u} + (s \leftrightarrow u), \quad (25)$$

that at high energy $s \gg m_\infty^2$ satisfies Eqs. (6a,6b) with $k_{\min} = 1$. By studying the pole structure of Eq. (25), one can see that the amplitude is mediated by states of any J with masses m_∞ , but also at $s = m_\rho$ we have now states with $J \neq 1$. Nevertheless, by taking the limit $m_\infty/m_\rho \rightarrow \infty$ in Eq. (25), we recover Eq. (24) as well as its low-energy predictions. So, as long as we are only interested in the Wilson coefficients, we can safely use Eq. (24).

At low energies, Eq. (24) leads to

$$g_{1,0} = 3 \frac{g_{\rho\pi\pi}^2}{m_\rho^2}, \quad g_{2,1} = \frac{4}{3} \frac{g_{1,0}}{m_\rho^2}, \quad g_{n,0} = \frac{1}{3} \frac{g_{1,0}}{m_\rho^{2n}}, \quad g_{n+1,1} = \frac{2}{3} \frac{g_{1,0}}{m_\rho^{2(n+1)}} \quad (n \geq 2), \quad (26)$$

while $g_{n,l} = 0$ for $l \geq 2$. Alternatively, we could compute the Wilson coefficients Eq. (26) from dispersion relations, by using the explicit form of the UV spectral density Eq. (9), with support on $J = 1$ and $m_i = m_\rho$ only. This can help us to appreciate the difference between $\mathcal{M}^{(\rho)}$ and its improved version $\widehat{\mathcal{M}}^{(\rho)}$. Indeed, since the vector amplitude Eq. (24) fulfils Eq. (6a) only for $k_{\min} \geq 2$, we can not use the sum rules Eq. (12) for $k_{\min} = 1$. In particular, the expressions for $g_{1,0}$ and $g_{2,1}$ from Eq. (13) do not hold – indeed they differ from those obtained directly from the amplitude Eq. (26). On the other hand, Eq. (24) fulfills Eq. (6b) for $k_{\min} = 1$ and one can use the prediction for $g_{2,1}$ from Eq. (15), that agrees with Eq. (26).

If instead we use $\widehat{\mathcal{M}}^{(\rho)}$ from Eq. (25) – which has $k_{\min} = 1$ high-energy behavior – the extra states beyond the ρ give a nonzero contribution to $g_{1,0}$ and $g_{2,1}$ that makes it to coincide with Eq. (26). These contributions tend to zero in Eq. (15).

²A more general function F in Eq. (21) would be associated with the exchange of longitudinal modes (contact terms to the Lagrangian) which would yield in the amplitude multiplicative factors $(s/m_\rho^2)^n$ that worsen the high-energy behavior.

2.3.3 Theory of spin-2 states

The pole structure of four-pion amplitude mediated by a spin-2 state only (in analogy with QCD we refer to it as f_2), can be written as,

$$\mathcal{M}^{(f_2)} = \frac{g_{f_2\pi\pi}^2 m_{f_2}^2}{m_{f_2}^2 - s} P_2 \left(1 + \frac{2u}{m_{f_2}^2} \right) + (s \leftrightarrow u). \quad (27)$$

Since $P_2(x) = (3x^2 - 1)/2$, this amplitude grows like $\sim s^2/u$ for large s , violating even the Froissart-Martin $k_{\min} = 2$ bound. Nevertheless, Eq. (27) can be deformed as in Eq. (25) to improve its high-energy behavior:

$$\widehat{\mathcal{M}}^{(f_2)} = \frac{g_{f_2\pi\pi}^2 m_{f_2}^2}{m_{f_2}^2 - s} P_2 \left(1 + \frac{2u}{m_{f_2}^2} \right) \frac{m_\infty^2}{m_\infty^2 - u} + (s \leftrightarrow u), \quad (28)$$

that indeed satisfies the Froissart-Martin bound for $s \gg m_\infty^2$, and leads to Eq. (27) in the limit $m_\infty/m_{f_2} \rightarrow \infty$. It is not possible to improve this further, as the resulting amplitude would have negative spectral density, and violates unitarity. For this reason amplitudes with light $J \geq 3$ (which grow as s^J from $P_J(1 + 2s/m_J^2)$) can not be completed into amplitudes that satisfy the Froissart-Martin bound, see also [32].

Contact terms (the function F in Eq. (21)) would modify Eq. (27). Nevertheless, demanding that they do not grow faster than Eq. (27), leaves only terms up to $O(s)$. These terms can only affect $g_{1,0}$, telling us that this Wilson coefficient cannot be predicted in a theory of spin-2 states. The rest of the Wilson coefficients, however, can be unambiguously derived from Eq. (27) in the low-energy limit:

$$\begin{aligned} g_{2,0} &= 7 \frac{g_{f_2\pi\pi}^2}{m_{f_2}^4}, & g_{2,1} &= \frac{12}{7} g_{2,0} = g_{3,1} m_{f_2}^2 = g_{4,2} m_{f_2}^4, & g_{n,0} &= \frac{1}{7} \frac{g_{2,0}}{m_{f_2}^{2n-4}} \quad (n \geq 3), \\ g_{n,1} &= \frac{6}{7} \frac{g_{2,0}}{m_{f_2}^{2n-4}} \quad (n \geq 4), & g_{n,2} &= \frac{6}{7} \frac{g_{2,0}}{m_{f_2}^{2n-4}} \quad (n \geq 5), \end{aligned} \quad (29)$$

with $g_{n,l} = 0$ for $l > 2$.

Similarly to the spin-1 case, we could calculate some of the Wilson coefficients from dispersion relations, with spectral density for $J = 2$ only. As Eq. (27) satisfies the high-energy limit Eqs. (6) for $k \geq k_{\min} = 3$, we can use the sum rules Eq. (12) with $k_{\min} = 3$ to obtain all the Wilson coefficients except $g_{1,0}$, $g_{2,0}$, $g_{2,1}$, $g_{3,1}$, $g_{4,2}$ and $g_{5,3}$ – indeed their value via Eq. (12) disagrees with Eq. (29). This can also be understood by realizing that the states of mass m_∞ present in the consistent amplitude Eq. (28) give finite contributions to $g_{1,0}$, $g_{2,0}$, $g_{2,1}$, $g_{3,1}$, $g_{4,2}$ and $g_{5,3}$ when Eq. (12) is used, even in the limit $m_\infty \rightarrow \infty$. For the coefficient $g_{3,1}$, however, we can alternatively determine it by using Eq. (16) that indeed agrees with Eq. (29).

2.3.4 The su -models

The su -models [6, 7] give the simplest four-pion amplitude mediated entirely by higher-spin states. The particularity of these models is that their spectrum is fully degenerate, $\mathcal{M}(s, u) \propto$

$1/(s - m^2)(u - m^2)$, a condition that naturally places these models at the boundary of the allowed parameter space, as we shall see. These su -amplitudes and the associated Wilson coefficients are discussed in detail in Appendix C.

2.3.5 The Lovelace-Shapiro and Coon amplitude

There are other four-pion amplitudes mediated by higher-spin states: the Lovelace-Shapiro [20, 21] amplitude and its generalization, the Coon amplitude [22]. These amplitudes originate in the context of string theory, and can provide therefore fully consistent UV completions to a theory of pions. We will see that the Wilson coefficients predicted by these amplitudes lie at the closest point to one of the boundaries of the allowed regions. Therefore they provide information about the mass spectrum of the theories residing on these boundaries. The details of these amplitudes are given in Appendices D and E.

3 Implications of $\mathcal{M}(s, u)/s \rightarrow 0$ at large s

In this section, we assume that the pion amplitude $\mathcal{M}(s, u)$ satisfies the conditions Eqs. (6a,6b) for $k_{\min} = 1$, as argued in Ref. [19]. Since all Wilson coefficients scale like $1/N_c$, and because positivity bounds are inherently projective (i.e. only ratios of Wilson coefficients are constrained), we will work with

$$\tilde{g}_{n,l} \equiv \frac{g_{n,l}}{g_{1,0}} M^{2(n-1)}, \quad (30)$$

where $g_{1,0}$ is the leading Wilson coefficient and M the EFT cutoff defined in Fig 1. Unless stated, we will take M as the lowest resonance mass. The $\tilde{g}_{n,l}$ are independent of N_c in the large- N_c limit.

We can use the sum rules Eq. (12) to determine the Wilson coefficients as a function of the mass spectrum, which is itself constrained by the null constraints. Our goal will be to shape the boundaries of the EFT parameter space, and identify the UV theories that generate it. When possible we shall use analytic arguments, complemented when necessary by numerics.

3.1 Bounds on the leading Wilson coefficients

Let us start by studying the implications of positivity bounds for $\pi\pi$ scattering at order $O(s^2)$, i.e. for the coefficients $g_{2,0}$ and $g_{2,1}$. As explained in Ref. [19], and recalled in Appendix A, the allowed regions can be obtained by numerical methods, see Fig. 3. These methods work extremely well as explorative tools and give conclusive answers when they rapidly approach known theories, e.g. [33]. Nevertheless, they are limited by computer power, and leave the question open of whether the extrapolation from finite resolution truly reveals a physically meaningful result. Here we will show that for some questions the numerical convergence is too slow, and we proceed by using analytic methods to map as much of the parameter space as possible.

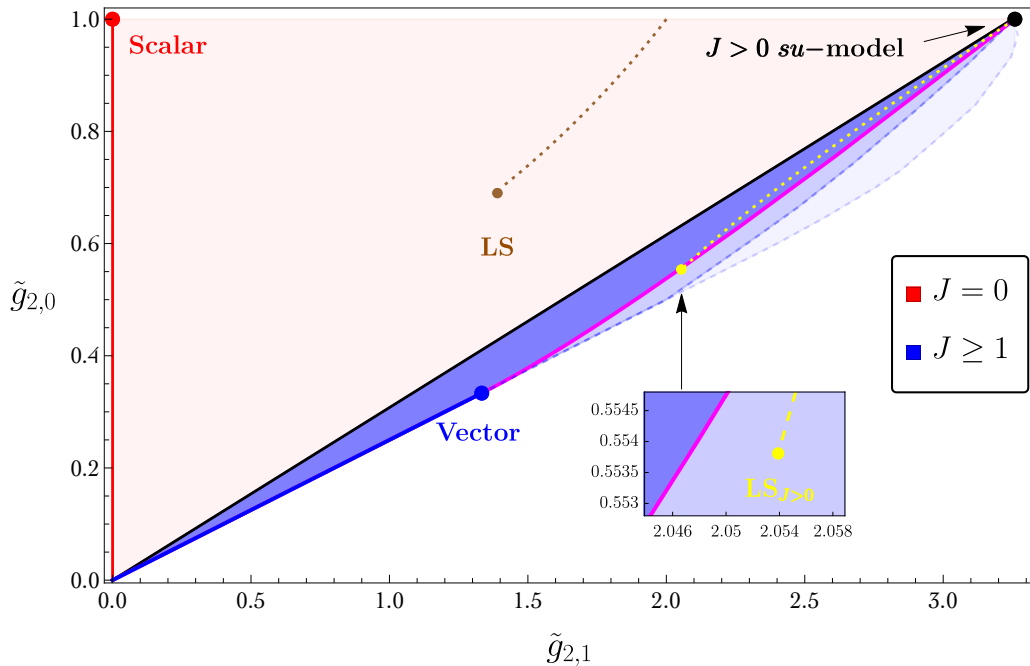


Figure 3: Allowed regions in the $\tilde{g}_{2,1}$ - $\tilde{g}_{2,0}$ plane, divided into regions with $J = 0$ states only (red line) and $J > 0$ states (blue) – using null constraints with $n_{\max} = 3$ (dashed light-blue line) and $n_{\max} = 11$ (dashed blue line). The dark blue area spans Eq. (47) for $0 \leq m_\rho \leq M$ and $m_\rho \leq m \leq \infty$. Moreover, $J = 1$ models lie on the blue line, $J > 0$ su -models on the black line (Eq. (92) with Eq. (94) and $0 \leq m \leq M$), and the magenta line corresponds to Eq. (48). The brown and yellow dot correspond to the Lovelace-Shapiro amplitude (Eq. (113)) respectively. The dashed brown and yellow line are the Coon amplitude (Eq. (118) with $C = 1$) with and without $J = 0$ states respectively.

Scalar theories and the $\tilde{g}_{2,1} > 0$ boundary. The smallest value of $\tilde{g}_{2,1} = 0$ is saturated by an amplitude mediated by $J = 0$ states, as discussed in section 2.3.1 – see also Ref. [19]. In particular, from Eq. (23), identifying $M = m_s$, we have $(\tilde{g}_{2,1}, \tilde{g}_{2,0}) = (0, 1)$, depicted as a red dot in Fig. 3. This point must clearly be a corner (kink) of the full allowed region, since from Eq. (13) one can see that $\tilde{g}_{2,1} \geq 0$ and $\tilde{g}_{2,0} \leq 1$. When more (non-degenerate) scalars are present, the value of $g_{2,0}/g_{1,0}$ always decreases, since $g_{2,0}$ scales as $\sim 1/m_s^4$ and therefore extra heavy scalars contribute more to $g_{1,0}$ than $g_{2,0}$ (the same is true for $g_{n,0}/g_{n-1,0}$). This is shown in Fig. 3 by a red line.

As discussed in section 2.1, states with $J < k_{\min}$ decouple from the null constraints. For $k_{\min} = 1$, only the $J = 0$ states decouple, meaning that it is the only simple theory that can provide a standalone UV completion of the chiral Lagrangian. All other UV completions must involve infinitely many states with all spins. It is therefore interesting to study the boundary of the region with $J \geq 1$ independently, as we discuss in what follows.

Spin-1 theories, the $\tilde{g}_{2,1}/\tilde{g}_{2,0} < 4$ boundary and its kink. The largest value of $\tilde{g}_{2,1}/\tilde{g}_{2,0}$ can be determined from Eq. (13) and Eq. (15), which gives

$$\frac{\tilde{g}_{2,1}}{\tilde{g}_{2,0}} = \frac{4 \langle \frac{1}{m^4} \rangle_{J\text{-odd}}}{\langle \frac{1}{m^4} \rangle_{J\text{-odd}} + \langle \frac{1}{m^4} \rangle_{J\text{-even}}}, \quad (31)$$

where the subscript denotes average over even or odd J only. This is saturated by $\tilde{g}_{2,1}/\tilde{g}_{2,0} = 4$ and corresponds to theories with only J -odd states. The simplest theory of this type is that described in Sec. 2.3.2 consisting of a light spin-1 state only, whose amplitude with the improved high-energy behavior is given in Eq. (25) with $m_\infty/m_\rho \rightarrow \infty$. From Eq. (26) we have

$$(\tilde{g}_{2,1}, \tilde{g}_{2,0})_{\text{vector}} = (4/3, 1/3), \quad (32)$$

shown in Fig. 3 as a blue dot. Adding extra spin-1 states allows us to move down from Eq. (32) to the origin, along the blue line of Fig. 3. This line must be part of the boundary of the allowed region for $(\tilde{g}_{2,1}, \tilde{g}_{2,0})$, since the ratio $\tilde{g}_{2,1}/\tilde{g}_{2,0} = 4$ takes the largest possible value.

The important question to address now is whether the allowed region can extend along the blue line beyond Eq. (32) or not. The numerical analysis of [19] was able to show that as one increases the number of null constraints, the kink moves towards Eq. (32), but appeared to tend asymptotically to a larger value. Here we will show that the kink resides at Eq. (32), i.e. the extremal theory along the boundary contains only a spin-1 light state.

To show this, we will first argue that at the boundary,

$$\tilde{g}_{2,0} = M^2 \frac{\langle \frac{1}{m^4} \rangle}{\langle \frac{1}{m^2} \rangle} \rightarrow M^2 \frac{\langle \frac{1}{m^4} \rangle_{J=1}}{\langle \frac{1}{m^2} \rangle_{J=1}} \frac{1}{1 + \frac{\langle \frac{1}{m^2} \rangle_{J>1}}{\langle \frac{1}{m^2} \rangle_{J=1}}}. \quad (33)$$

This can be proven as follows. Eq. (31) implies that at the boundary even- J states must decouple from the average in $g_{2,0}$,

$$\langle \frac{1}{m^4} \rangle_{J\text{-even}} \rightarrow 0. \quad (34)$$

Using the Cauchy-Schwarz inequality (where $\langle \mathcal{J}^4/m^8 \rangle$ must be finite because it enters in the null constraint in the first expression of Eq. (19)), we have

$$\sqrt{\langle \frac{\mathcal{J}^4}{m^8} \rangle_{J\text{-even}} \langle \frac{1}{m^4} \rangle_{J\text{-even}}} \geq \langle \frac{\mathcal{J}^2}{m^6} \rangle_{J\text{-even}} \rightarrow 0. \quad (35)$$

This, together with the null constraint $\langle \mathcal{Y}_{3,1} \rangle = 0$ Eq. (20), implies,

$$\langle \frac{\mathcal{J}^2}{m^6} \rangle_{J\text{-even}} = 3 \langle \frac{\mathcal{J}^2 - 2}{m^6} \rangle_{J\text{-odd}} \geq 12 \langle \frac{1}{m^6} \rangle_{J>1\text{-odd}} \rightarrow 0, \quad (36)$$

because $\mathcal{J}^2 - 2 = 0$ on $J = 1$ and $\mathcal{J}^2 - 2 \geq 4$ for $J \geq 2$. Using Cauchy-Schwarz again (with measure on odd $J > 1$ only), and the fact that $\langle \frac{1}{m^2} \rangle_{J>1\text{-odd}}$ is finite, we find

$$\sqrt{\langle \frac{1}{m^6} \rangle_{J>1\text{-odd}} \langle \frac{1}{m^2} \rangle_{J>1\text{-odd}}} \geq \langle \frac{1}{m^4} \rangle_{J>1\text{-odd}} \rightarrow 0, \quad (37)$$

thus proving Eq. (33). The theory that lives on the boundary must therefore consist of spin-1 states at finite mass accompanied by higher-spin states at infinite mass.

Unfortunately, this is not yet enough to claim that it is *exactly* the theory in Eq. (25), since there might be different ways in which the $J \rightarrow \infty$ states enter in the spectral density.

To prove that it is, we reformulate the question of finding the maximum value of the kink, as a 1D moment problem. Indeed, the kink is positioned at the maximum value of $\tilde{g}_{2,0}$ along the boundary given by Eq. (33). The first factor $\langle \frac{1}{m^4} \rangle_{J=1} / \langle \frac{1}{m^2} \rangle_{J=1} \leq 1$ is maximally saturated when the spectrum contains only one spin-1 particle at the mass M , $M^2 \langle \frac{1}{m^4} \rangle_{J=1} = \langle \frac{1}{m^2} \rangle_{J=1} \equiv g_{\rho\pi\pi}^2 / M^2$. Then, from the second factor in Eq. (33) we read that the kink is located at the *minimum* of,

$$\frac{M^2}{g_{\rho\pi\pi}^2} \left\langle \frac{1}{m^2} \right\rangle_{J>1}. \quad (38)$$

This minimum cannot be zero, because the null constraints relate the high-energy averages to $g_{\rho\pi\pi}^2$, in such a way that the ratio is finite. Indeed, along the boundary, the dominant null constraints Eq. (18) can be written as,

$$2(n-1)!^2 = \frac{M^{2n}}{g_{\rho\pi\pi}^2} \left\langle \frac{J^{2(n-1)}}{m^{2n}} \right\rangle_{J>1}, \quad n = 2, 3, 4, \dots, \quad (39)$$

i.e. all subleading terms J^k with $k < 2(n-1)$ can be neglected. This can be understood from the comment below Eq. (37) – for states with infinite mass, if in the average $\lim_{m \rightarrow \infty} J^{2(n-1)} / m^{2n}$ is finite, then all subleading powers of J must vanish.³ With a change of variables to (the square of) impact parameter $x \equiv J^2 M^2 / m^2$, and redefining n , we can write Eq. (39) as

$$2n!^2 = \int_0^\infty d\mu(x) x^n dx \equiv \mu_n, \quad n = 1, 2, 3, \dots, \quad (41)$$

with $d\mu(x)$ a positive distribution. In this language Eq. (38) is μ_0 , and the problem of finding the kink position translates into a 1-dimensional moment problem:

finding the minimum of μ_0 such that $\{\mu_0, \mu_1, \mu_2, \dots\}$ is a moment series from a positive distribution, with $\mu_n = 2n!^2$ for $n \geq 1$. (42)

A sufficient condition for this, is that the Hankel matrix H_N^0 , with $(H_N^k)_{ij} = \mu_{i+j+k}$, for

³It can also be seen by using the Hölder inequality and $\langle 1/m^{2k} \rangle_{J>1} \rightarrow 0$ (for $k \geq 1$) from Eq. (37),

$$\left\langle \frac{1}{m^{2k}} \right\rangle_{J>1}^{\frac{1}{k}} \left\langle \frac{J^{2(n-k-1)}}{m^{2(n-k)}} \right\rangle_{J>1}^{1-\frac{1}{k}} \geq \left\langle \frac{J^{2(n-k-1)}}{m^{2n}} \right\rangle_{J>1} \rightarrow 0. \quad (40)$$

$i, j = 0, \dots, \lfloor N/2 \rfloor$, be asymptotically positive definite [4, 34],

$$\lim_{N \rightarrow \infty} H_N^0 = 2 \lim_{N \rightarrow \infty} \begin{pmatrix} \mu_0/2 & 1!^2 & 2!^2 & \dots & n!^2 \\ 1!^2 & 2!^2 & 3!^2 & \dots & (n+1)!^2 \\ 2!^2 & 3!^2 & 4!^2 & \dots & (n+2)!^2 \\ \dots & \dots & \dots & \ddots & \vdots \\ n!^2 & (n+1)!^2 & (n+2)!^2 & \dots & (2n)!^2 \end{pmatrix} \succ 0. \quad (43)$$

Equivalently (using Sylvester's criterion) this can be rewritten as,

$$1 - \mu_0/2 \leq \lim_{N \rightarrow \infty} \frac{\det H_N^0|_{\mu_0=1}}{\det H_N^2}. \quad (44)$$

Explicit evaluation of Eq. (44) for fixed N enables us to reach smaller and smaller values, going from $\mu_0 \approx 0.95$ for $N = 10$ (equivalent to $\tilde{g}_{2,0} \approx 0.51$) to $\mu_0 \approx 1.54$ for $N = 700$ (equivalent to $\tilde{g}_{2,0} \approx 0.39$) – to be compared with $\tilde{g}_{2,0} \approx 0.42$ of Ref. [19]. Computing the asymptotic behavior of determinants of this type is an interesting open problem in mathematics, see e.g. [35], motivated by their appearance in random matrix theory (interestingly, also in relation with QCD and chiral perturbation theory [36, 37]). Leaving this for future work, in Appendix B we take a shortcut and, rather than computing the individual determinants, we focus on the most efficient way of computing the ratio Eq. (44), and show that as $n \rightarrow \infty$,

$$\mu_0 \rightarrow 2 \quad \text{and} \quad (\tilde{g}_{2,1}, \tilde{g}_{2,0}) \rightarrow (4/3, 1/3). \quad (45)$$

At the kink resides the theory of a single spin-1 state, with the improved high-energy behavior amplitude Eq. (25) with $m_\infty \gg m_\rho$.

The su -model and the boundary for $J \geq 1$ with minimal $\tilde{g}_{2,1}/\tilde{g}_{2,0}$. At the largest value of $\tilde{g}_{2,0} = 1$ must lie theories with a degenerate spectrum, see Eq. (13). Apart from a theory of a scalar (discussed before), the only amplitude with this property is the su -model discussed in Appendix C, with amplitude Eq. (92). This amplitude can also be obtained analytically by solving the null constraints. Indeed, for a degenerate spectrum, the null constraints reduce to a system of equations for the couplings $g_{i\pi\pi}^2$. The dominant null constraints Eq. (18), for instance, are linearly independent, and can be solved explicitly for a fixed number of couplings $g_{i\pi\pi}^2$ with $i = 1, \dots, n$. The solution is a function that can be resummed and converges into the su -model prediction.

This su -model contains a fraction of scalar residues, controlled by the value of λ in Eq. (93); for the value in Eq. (94) the theory has no scalars. Its amplitude lies at,

$$(\tilde{g}_{2,1}, \tilde{g}_{2,0})_{J>0 \text{ } su\text{-model}} = (\approx 3.26, 1), \quad (46)$$

shown by the black dot in Fig. 3. The uniqueness of this amplitude naturally puts it at kink of the $J \geq 1$ region (and its linear combination with the scalar amplitude at the boundary of the $J \geq 0$ region).

As the spectrum becomes heavier, $M/m \rightarrow 0$, the su -model morphs into the free theory (at the origin of the plot in Fig. 3). Interestingly, this line defines the boundary of the allowed region for theories characterised by resonances of spin $J \geq 1$. In Appendix C we show that this line is indeed a boundary by considering the most generic deformation of the su -model and showing that in order to not spoil positivity these deformations must push you in the bulk of the exclusion region (excluding the contribution from scalars).

Boundary between kinks. Therefore we are left with the boundary line joining the two kinks, Eq. (32) and Eq. (46). We have not found an analytical expression for this curve. Nevertheless, as proposed in Ref. [19], we can have a reasonable analytical formula by considering a model that interpolates between a spin-1 model and the $J > 0$ su -model. The interpolating amplitude is given by⁴

$$\mathcal{M} = \mathcal{M}_1^{(su)} - \frac{3(\ln 8 - 2)}{g_{\rho\pi\pi}^2} \left(\widehat{\mathcal{M}}^{(\rho)}(m_\rho \rightarrow m) - \widehat{\mathcal{M}}^{(\rho)} \right), \quad (47)$$

which corresponds to a $J > 0$ su -model in which the spin-1 state of mass m has been subtracted and replaced by a spin-1 state of mass m_ρ . We have used the corrected amplitude $\widehat{\mathcal{M}}^{(\rho)}$ from Eq. (25), to assure that Eq. (47) satisfies the high-energy conditions with $k_{\min} = 1$ for all values of its parameters; nevertheless we will be taking the limit $m_\infty/m_\rho \rightarrow \infty$ that corresponds to $\widehat{\mathcal{M}}^{(\rho)} \rightarrow \mathcal{M}^{(\rho)}$. From Eq. (47) it is clear that by varying the mass m from m_ρ to infinity, we are effectively pushing up the masses of the $J > 1$ states in the su -model, leaving only a $J = 1$ state at low energy. The corresponding Wilson coefficients of Eq. (47) can be easily calculated and one obtains, for $M = m_\rho$,

$$\tilde{g}_{2,0} = \frac{a - (3 - 10a)(r^2 - 1)}{a - (9 - 28a)(r - 1)}, \quad \tilde{g}_{2,1} = \frac{1 + (36a - 11)(r^2 - 1)}{a - (9 - 28a)(r - 1)}, \quad (48)$$

where $r = m_\rho^2/m^2$ and $a = 1 - \ln 2$. The magenta line in Fig. 3 is obtained by varying $r \in [0, 1]$.

We have determined this boundary numerically (following Ref. [19], see our Appendix A for details), including null constraints with $n_{\max} = 3$ and $n_{\max} = 11$, shown by dashed lines in Fig. 3. Due to the lack of computational power, however, we have not been able to understand how much the true boundary approaches the analytic boundary Eq. (48) as $n \rightarrow \infty$. Nevertheless, we can claim that Eq. (48) cannot coincide with the true bound, as we know of another consistent amplitude that lies on the RHS of this line. This is the Lovelace-Shapiro amplitude in which the scalar contribution has been removed (see Appendix D for details). The prediction for this amplitude (see Eq. (115)) is shown by a yellow dot in Fig. 3. In spite of this, the prediction of this amplitude is impressively close to Eq. (47) as can be appreciated by the zoom area in Fig. 3. We also show a version of the scalar-subtracted Coon amplitude, Eq. (118) in Appendix E, with $C = 1$ and q varied from 0 to 1. This line starts at the $J > 0$ su -model and goes down to the Lovelace-Shapiro model. It slightly improves Eq. (48) but only close to the Lovelace-Shapiro

⁴There are other possible interpolating amplitudes, but Eq. (47) is the one with the smallest number of states that we have found. Adding more states will give predictions for $(\tilde{g}_{2,1}, \tilde{g}_{2,0})$ that will lie on the left of the magenta line of Fig. 3.

values ($q \simeq 1$). It could be interesting to know if there is another deformation of the Lovelace-Shapiro amplitude that saturates the true boundary. We also show in Fig. 3 the prediction from the full Lovelace-Shapiro and Coon amplitudes (with $C = 1$) without subtracting the scalar contributions.

For models with both $J = 0$ and $J > 0$ states, the allowed region corresponds to the convex hull spanned by the individual boundaries, shown in light red (plus blue) in Fig. 3.

3.2 Emergence of Vector Meson Dominance

We have seen that a theory of a spin-1 state does not satisfy $\mathcal{M}(s, u)/s \rightarrow 0$ at large s , fixed $u < 0$, and requires higher-spin states to soften the high-energy behavior. The converse is also true: any model of higher-spin states must contain spin-1 mesons. This can be made explicit by looking at null constraints. For example, the first two null constraints, $\langle \mathcal{Y}_{2,1} \rangle = 0$ and $\langle \mathcal{X}_{3,1} \rangle = 0$ of Eq. (18), lead to

$$\begin{aligned} \left\langle \frac{1}{m^4} \right\rangle \Big|_{J=1} &= 3 \left\langle \frac{1}{m^4} \right\rangle \Big|_{J=2} + 4 \left\langle \frac{1}{m^4} \right\rangle \Big|_{J=3} + \dots, \\ \left\langle \frac{1}{m^6} \right\rangle \Big|_{J=1} &= 9 \left\langle \frac{1}{m^6} \right\rangle \Big|_{J=3} + 35 \left\langle \frac{1}{m^6} \right\rangle \Big|_{J=4} + \dots. \end{aligned} \quad (49)$$

Since the RHS is always positive, this identity can only be fulfilled if there are spin-1 states in the theory. These equations also tell us that, at any order in $1/m^n$ in the average, the contributions from any individual $J > 1$ state must always be smaller than the ρ contribution, since the coefficients appearing on the RHS are always bigger than one. Moreover, these coefficients scale with large J as $\sim J^{2n-2}/m^{2n}$, which is faster than how they appear in the low-energy couplings such as $g_{n,0} \sim \langle 1/m^{2n} \rangle$ or $g_{n,1} \sim \langle J^2/m^{2n} \rangle$ (but $g_{2,1} \sim \langle 1/m^4 \rangle$) from Eq. (12).⁵

The property that the ρ meson dominates the low-energy amplitude of pions (or at least that amplitudes with ρ mesons populate the space of consistent pion amplitudes) is referred to as Vector Meson Dominance (VMD) [23, 24]. Despite its poor theoretical motivation, VMD is known to lead to good agreement with QCD experimental data. Here we see that VMD emerges from unitarity and crossing symmetry. For the most relevant couplings, it is illustrated by the alignment between the $J > 0$ allowed region and the spin-1 line observed in Fig. 4. The QCD experimental value, as determined in Ref. [38], is denoted by the red cross in the figure.

As the masses of the $J > 1$ states increase, VMD becomes more manifest. Indeed, from Eqs. (13,15), the contributions from the high-spin states at large mass $m_{J>1} \rightarrow \infty$ go as,

$$\frac{g_{2,0}}{g_{1,0}} \sim \frac{g_{2,1}}{g_{1,0}} \sim \frac{1}{m_{J>1}^2} \rightarrow 0,$$

while the $J = 1$ contribution remains finite. This is also true for the rest of the Wilson coefficients, since for large scale separations between the ρ and higher spins $m_\rho/m_{J>1} \rightarrow 0$, The

⁵For couplings $g_{n,l}$ with larger and larger l this argument is more involved, since the $J = 1$ contribution cancels from Eq. (12) and is restored only via null constraints.

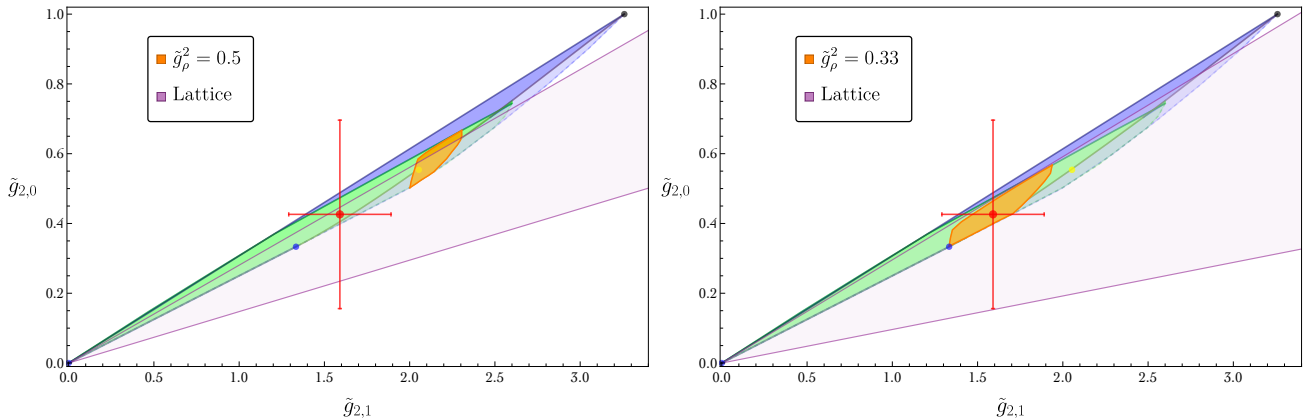


Figure 4: Allowed regions from positivity with $J \geq 1$ (as in Fig. 3). The green regions have heavier resonances of all spin $J \geq 1$ with masses $M' \geq 1.65 m_\rho$: the dashed green line uses null constraints up to $n_{\max} = 11$. In orange the allowed region for a fixed $\tilde{g}_\rho = 1/2$ (left) and $\tilde{g}_\rho = 1/3$ (right), with still $M'/m_\rho = 1.65$. In purple, the allowed region from Lattice simulations [39–41]. In red the QCD experimental value from Ref. [38].

null constraints Eq. (18) require a finite contribution from the $J \rightarrow \infty$ states, in such a way that $J^2/m_{J>1}^2$ remains fixed in units of $g_{1,0} \sim 1/m_{J>1}^2$. Using Eq. (13), this implies that the $J > 1$ contribution to the Wilson coefficients scales as,

$$\Delta g_{n+l,l} \sim \frac{J^{2l}}{m_{J>1}^{2(n+l)}} \sim \frac{1}{m_{J>1}^{2n}}, \quad (50)$$

and therefore tends to zero for large $m_{J>1}$.

At finite masses, we can study this effect numerically, requiring a finite mass gap between the ρ meson and other resonances $M' > m_\rho$, i.e. we work with the spectral density [19],

$$(2J+1)\rho_J(s) \rightarrow \frac{\pi}{2} g_{\rho\pi\pi}^2 \delta_{J,1} \delta(s - m_\rho^2) + (2J+1)\rho'_J(s), \quad (51)$$

where the last term corresponds to extra states with $s \in [M', \infty)$ (see Appendix A). In QCD, the lightest higher-spin resonance is a spin-2 meson f_2 with a mass $m_{f_2} \approx 1.3$ GeV, which implies $M'/m_\rho \sim 1.65$. With this mass gap, the allowed region reduces to the small green strip in Fig. 4, which is more strongly aligned with the spin-1 prediction, evidencing VMD.

It is instructive to further divide the allowed region of parameters in terms of the contribution of the ρ to the leading Wilson coefficient $g_{1,0}$, i.e.

$$\tilde{g}_\rho^2 \equiv \frac{g_{\rho\pi\pi}^2}{g_{1,0} m_\rho^2}, \quad (52)$$

which can be thought to quantify VMD. In Fig. 4 we show in orange the allowed regions in which \tilde{g}_ρ^2 matches the experimental QCD value and the value taken in the vector model Eq. (24),

$$(a) \tilde{g}_\rho^2 \simeq \frac{1}{2} \quad (\text{QCD}), \quad (b) \tilde{g}_\rho^2 = \frac{1}{3} \quad (\text{spin-1 model}). \quad (53)$$

As we will discuss in Sec. 3.4, $\tilde{g}_\rho^2 = 1/2$ is close to its maximal value $\tilde{g}_\rho^2 \sim 0.78$, which is also where the associated spectral density has the $J > 1$ contributions maximised (saturated by the su -model). On the other hand, even for $\tilde{g}_\rho^2 = 1/3$ (for which $2/3$ of the leading effects are taken care by higher spin-mesons), the allowed region for $\tilde{g}_{2,0}$ and $\tilde{g}_{2,1}$ still sits close to the spin-1 contribution (blue dot), showing a small effect from the $J > 1$ states.

Our discussion of VMD so far focused on quantifying the contributions from $J > 1$ mesons: these are the difficult ones to model, and for which our arguments are particularly important. On the other hand, since $J = 0$ states decouple from the null constraint, they could indeed dominate $\tilde{g}_{2,0}$ and $\tilde{g}_{2,1}$, as it happens in the Higgs model. Nevertheless, scalars can be easily accommodated in any phenomenological analyses as they have simple UV completions. It is worth noticing, however, that when a spin-1 ρ is assumed to be the lightest meson in the spectrum, as in QCD, the scalar contribution becomes smaller. This property is tied to the fact that contributions to the Wilson coefficients are always positive. For example, taking scalars with masses $\gtrsim 1.65 m_\rho$, while still fixing \tilde{g}_ρ^2 to the values considered above, we find that the resulting allowed regions depicted in Fig. 4 increase in size by only 10 – 25% along the $\tilde{g}_{2,0}$ direction.

3.2.1 Comparison with Lattice QCD

The Wilson coefficients $L_{1,2,3}$, traditionally defined in the $SU(3)$ chiral Lagrangian [42],⁶ are related to ours by

$$\tilde{g}_{2,0} = 4(2L_1 + 3L_2 + L_3) \frac{M^2}{F_\pi^2}, \quad \tilde{g}_{2,1} = 16L_2 \frac{M^2}{F_\pi^2}. \quad (54)$$

In the large- N_c limit, $2L_1 = L_2$ [42], which leads to

$$\frac{\tilde{g}_{2,0}}{\tilde{g}_{2,1}} = \frac{1}{4} \left(1 + \frac{\Delta_L}{L_2} \right), \quad (55)$$

where $\Delta_L = 3L_2 + L_3$. This quantity vanishes for theories with only spin-1 resonances, so VMD predicts $\Delta_L \sim 0$. Moreover, the positivity of the Wilson coefficients implies that $L_2, \Delta_L \geq 0$.

A combination of recent lattice simulation results for large- N_c QCD [39–41], gives $\Delta_L = (-0.12 \pm 0.22) \cdot 10^{-3}$. Unfortunately, we have not found any lattice determination of L_2 . Nevertheless, for any given value of \tilde{g}_ρ , we have a minimal value for $L_2 \propto g_{2,1}$, which plugged into Eq. (55) with the lattice value of Δ_L , can provide a bound on $\tilde{g}_{2,0}/\tilde{g}_{2,1}$. For the two values of Eq. (53), we find

$$(a) \ 0.15 \lesssim \frac{\tilde{g}_{2,0}}{\tilde{g}_{2,1}} \lesssim 0.28, \quad (b) \ 0.10 \lesssim \frac{\tilde{g}_{2,0}}{\tilde{g}_{2,1}} \lesssim 0.30, \quad (56)$$

⁶Following the chiral Lagrangian definition in Ref. [42],

$$\mathcal{L} = \frac{F_\pi^2}{4} \text{Tr} (\partial_\mu U^\dagger \partial^\mu U) + L_1 \text{Tr}^2 (\partial_\mu U^\dagger \partial^\mu U) + L_2 \text{Tr} (\partial_\mu U^\dagger \partial_\nu U) \text{Tr} (\partial^\mu U^\dagger \partial^\nu U) + L_3 \text{Tr} (\partial_\mu U^\dagger \partial^\mu U \partial_\nu U^\dagger \partial^\nu U).$$

that correspond to the purple areas in Fig. 4. We notice that in both cases positivity bounds are complementary to bounds from lattice, ruling out different regions. In the particular case (a), the upper bound coming from lattice seems to be more restrictive than the one from positivity, but this is not the case as we decrease \tilde{g}_ρ^2 . In the future a combination of both approaches can lead to a better determination of the geometry of the allowed regions in parameter space.

3.2.2 Holography

The results in Figs. 4 provide also an explanation for the success of holography for predicting QCD properties [25, 26]. Holographic models consist in weakly-coupled 5D constructions describing 4D strongly-coupled dynamics in both the $N_c \rightarrow \infty$ limit, and the limit of a large mass gap between spin-0,1 states and other higher-spin states.⁷

In real QCD, however, the mass ratio between the $q\bar{q}$ mesons of spin-2 and spin-1 is not large, $m_{f_2}/m_\rho \sim 1.65$. Therefore, one would expect holographic models not to provide a good description of low-energy QCD, contrary to what is observed [25, 26]. Nevertheless, the above analysis shows that unitarity, causality and crossing-symmetry suppress the effects of higher-spin states in the QCD Wilson coefficients. Therefore, even if the mass gap m_{f_2}/m_ρ is not large, the low-energy QCD quantities are mostly affected by only spin-0 and spin-1 states, which are the ones captured by holographic models. For this reason they can provide a good fit to real-world QCD.

In particular, in the holographic model of Ref. [43], one can show that the predictions for $\tilde{g}_{2,0}$ and $\tilde{g}_{2,1}$ are very close to those of the vector model $(\tilde{g}_{2,1}, \tilde{g}_{2,0}) = (1.32, 0.33)$.

3.3 Higher order Wilson coefficients

The features that sculpt the allowed region of $\tilde{g}_{2,0}$ and $\tilde{g}_{2,1}$ play a dominant role also in understanding higher-order Wilson coefficients, $\tilde{g}_{n,0}$ versus $\tilde{g}_{n,1}$. From Eq. (13) we have,

$$\frac{\tilde{g}_{n,1}}{\tilde{g}_{n,0}} = \frac{\langle \frac{\mathcal{J}^2}{m^{2n}} \rangle}{\langle \frac{1}{m^{2n}} \rangle}, \quad (57)$$

whose minimal value (zero) corresponds to a model with $J = 0$. Focusing instead on $J > 0$ theories, the minimal value arises for models of spin-1 that give $\tilde{g}_{n,1}/\tilde{g}_{n,0} = 2$.⁸

We illustrate this in Fig. 5, where a blue dot corresponds to a model with a single $J = 1$ state:

$$(\tilde{g}_{3,1}, \tilde{g}_{3,0})_{\text{vector}} = (2/3, 1/3), \quad (58)$$

while theories with many spin-1 states populate the blue line.

⁷The model also has 5D gravitons, but these correspond to glueballs of spin $J \leq 2$, which decouple from the pion amplitudes.

⁸Notice that we could not use this argument for the case $n = 2$, since we cannot use the sum rules in Eq. (57) with $n = 2$ for a theory of $J = 1$ states only, as explained at the end of Sec. 2.3.2. In other words, the infinitely heavy $J > 1$ states give zero contribution to Eq. (57) only when $n > 2$.

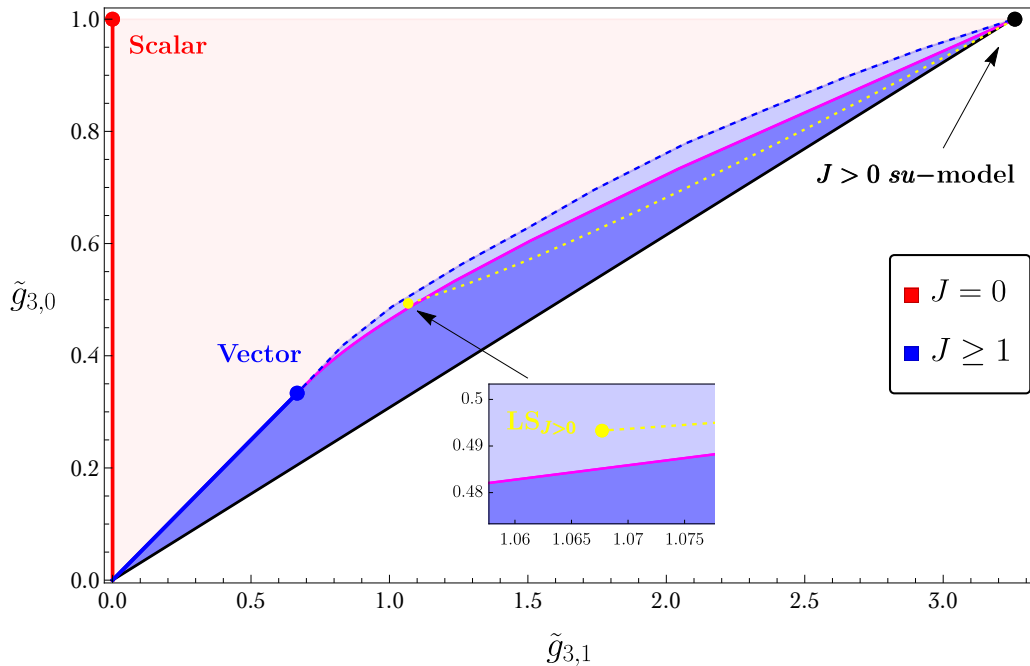


Figure 5: Allowed region in the $\tilde{g}_{3,1}$ - $\tilde{g}_{3,0}$ plane from positivity. Same labelling as in Fig. 3, with $n_{\max} = 11$ null constraints.

As for $\tilde{g}_{2,0}, \tilde{g}_{2,1}$, we can show that Eq. (58) corresponds to a kink of the boundary, see Appendix B. The other kink corresponds again to the $J > 0$ su -model (the only one with a degenerate spectrum) that gives

$$(\tilde{g}_{3,1}, \tilde{g}_{3,0})_{su\text{-model}} = (\approx 3.26, 1). \quad (59)$$

We have not been able to find an analytic formula for the boundary connecting the two kinks, Eq. (58) and Eq. (59); we illustrate the numerical analysis in Fig. 5. We believe that by adding more null constraints the boundary must approach, but not reach, Eq. (47), consisting of a theory connecting the two kinks (the magenta line in Fig. 5). Nevertheless, as in Sec. 3.1, this line cannot be the true boundary since the Lovelace-Sphapiro model with $J > 0$ states lies at the left of this line, and so does part of the Coon amplitude, Eq. (118) (with $C = 1$ and $q \in [0, 1]$, after subtracting all scalars).

3.4 Bounding the couplings of mesons to pions

So far, we have phrased dispersion relations as UV \rightarrow IR vehicles to reformulate microscopic unitarity, causality and crossing-symmetry as predictions for low-energy coefficients. Null constraints, however, provide genuine UV-UV relations, inspired by the same principles. As such, they contain information on the UV meson spectrum and couplings to pions. We define the latter, normalized as,

$$\tilde{g}_i^2 = \frac{g_{i\pi\pi}^2}{g_{1,0} m_i^2}, \quad (60)$$

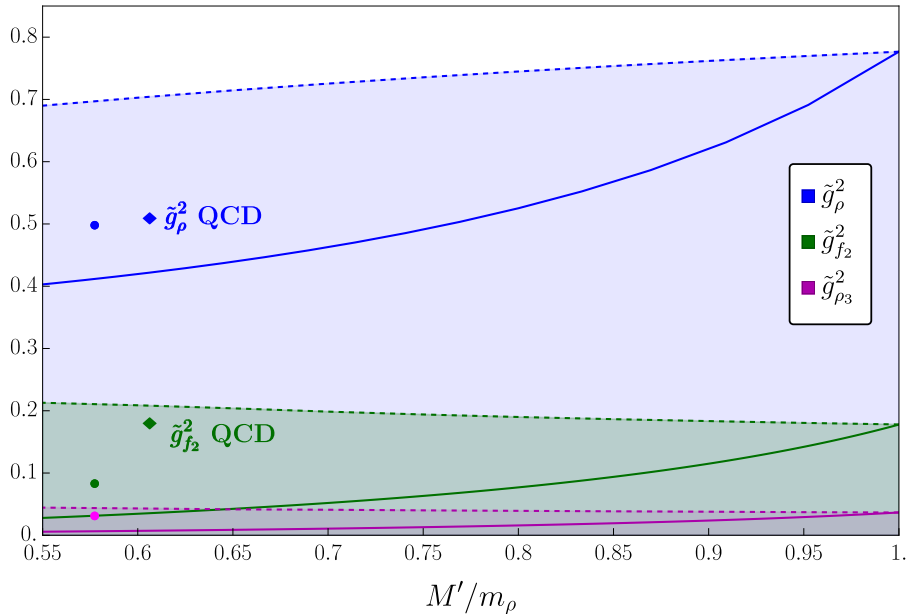


Figure 6: Upper bound on \tilde{g}_ρ^2 (dashed blue line), $\tilde{g}_{f_2}^2$ (dashed green line) and $\tilde{g}_{\rho_3}^2$ (dashed magenta line) as a function of M'/m_ρ using null constraints with $n_{\max} = 7$. The solid lines correspond to the prediction from the interpolating model Eq. (47). The dots correspond to the values of the Lovelace-Shapiro amplitude without scalars, and the diamonds to the QCD experimental values.

where $i = s, \rho, f_2, \rho_3, \dots$ labels $J = 0, 1, 2, 3, \dots$ mesons, following the QCD notation of Ref. [44].

Since spin-0 mesons decouple from the null constraints, it is easy to understand that \tilde{g}_s^2 is maximised by the smallest possible value of $g_{1,0}$ that, due to its additive property, occurs when the spectrum contains one scalar only:

$$\tilde{g}_s^2 \leq 1. \quad (61)$$

On the other hand, bounds on the couplings of $J \geq 1$ mesons, involve all null constraints, which we explore numerically, as explained in Appendix A. The results are illustrated in Fig. 6. For instance, the bound on the ρ coupling \tilde{g}_ρ^2 (dashed blue line), is obtained as a function of $M' \geq m_\rho$ by singling out this state from the spectral density as in Eq. (51). The bound goes from a maximal value $\tilde{g}_\rho^2 \simeq 0.78$, corresponding to the $J > 0$ su -model where $M' = m_\rho$, to the minimal value corresponding to the vector model, $\tilde{g}_\rho^2 = 1/3$ where $M' \rightarrow \infty$. This can be compared with the interpolating model Eq. (47) shown by the solid blue line and with the Lovelace-Shapiro model without scalars Eq. (113) (shown by dots) that lies between the two lines. Interestingly, while all these models give similar predictions in terms of the Wilson coefficients – see Fig. 3 – they differ substantially at the quantitative level in Fig. 6. This provides an interesting experimental handle to differentiate these theories by testing the couplings of pions to the accessible resonances (amplitude’s residues).

Similarly for the spin-2 meson f_2 , we rewrite the spectral density as,

$$(2J + 1)\rho_J(s) \rightarrow \frac{\pi}{2}g_{\rho\pi\pi}^2\delta_{J,1}\delta(s - m_\rho^2) + \frac{\pi}{2}g_{f_2\pi\pi}^2\delta_{J,2}\delta(s - M'^2) + (2J + 1)\rho'_J(s), \quad (62)$$

and look for the upper bound on $\tilde{g}_{f_2}^2$ as a function of M'/m_ρ for any value of $g_{\rho\pi\pi}^2 > 0$. This is shown by the green dashed line in Fig. 6. The resulting bound is much stricter than that for the ρ – another manifestation of VMD.

As we study mesons of higher and higher spin J , the bound on \tilde{g}_i^2 becomes stronger and stronger – see the magenta dashed line for $\tilde{g}_{\rho_3}^2$. Interestingly, this pattern is also tracked by the QCD experimental values, $\tilde{g}_\rho^2 = 0.51 \pm 0.01$ and $\tilde{g}_{f_2}^2 = 0.18 \pm 0.01$, extracted from the widths $\rho, f_2 \rightarrow \pi\pi$ [44], as shown by the diamonds in Fig. 6.

4 Implications of $\mathcal{M}(s, u)/s^2 \rightarrow 0$ at large s

A more conservative assumption is that the four-pion amplitude satisfies the Froissart-Martin bound, Eqs. (6a,6b) for $k_{\min} = 2$, rather than $k_{\min} = 1$ as in the previous section. Unfortunately in this case we lose the sum rule for the Wilson coefficient $g_{1,0}$ (and $g_{2,1}$ is no longer expressible by Eq. (12) – which comes from $k_{\min} = 1$ – but requires Eq. (15)). So, we will need to choose another Wilson coefficient to normalize the rest and make the predictions N_c -independent. We will use $g_{2,0}$ and define,

$$\bar{g}_{n,l} \equiv \frac{g_{n,l}}{g_{2,0}} M^{2(n-2)}. \quad (63)$$

There is another important difference w.r.t. Sec. 3. The amplitude mediated by a spin-1 state, Eq. (24), fulfils $\mathcal{M}^{(\rho)}/s^2 \rightarrow 0$ for large $|s|$, and therefore now provides a good UV description of the four-pion amplitude. As a consequence, models of spin-1 states do not require anymore higher-spin states. From the perspective of null constraints this is realised by the decoupling of $J = 1$, when setting $k_{\min} = 2$, as we explained in Sec. 2.1

It is the spin-2 state that now plays an analog role to that of the ρ -meson in Sec. 3. Indeed, the $\langle \mathcal{Y}_{4,2} - \mathcal{Y}_{4,1} \rangle = 0$ null constraint reads,

$$6 \left\langle \frac{1}{m^8} \right\rangle \Big|_{J=2} = 10 \left\langle \frac{1}{m^8} \right\rangle \Big|_{J=3} + 50 \left\langle \frac{1}{m^8} \right\rangle \Big|_{J=4} + \dots, \quad (64)$$

which tells us that spin-2 states need $J > 2$ states and viceversa (for instance, the amplitude Eq. (27) requires $J \geq 3$ states as in Eq. (28), to comply with the Froissart-Martin bound).

4.1 Bounds on Wilson coefficients

At the leading order $O(s^2)$, we only have $\bar{g}_{2,1}$. As discussed before, we have $\bar{g}_{2,1} = 0$ ($\bar{g}_{2,1} = 4$) for $J = 0$ ($J = 1$) models, that are decoupled from higher-spin states. Focusing instead on theories with $J \geq 2$ states, the largest value of $\bar{g}_{2,1}$ comes from the su -model, once we have subtracted not only the scalar but also the $J = 1$ state, whose amplitude is given by Eq. (97) in appendix C, using Eq. (98). Then, from Eq. (100) we find,

$$\bar{g}_{2,1} \leq \frac{18 \ln 2 - 13}{10 \ln 2 - 7} \simeq 7.6. \quad (65)$$

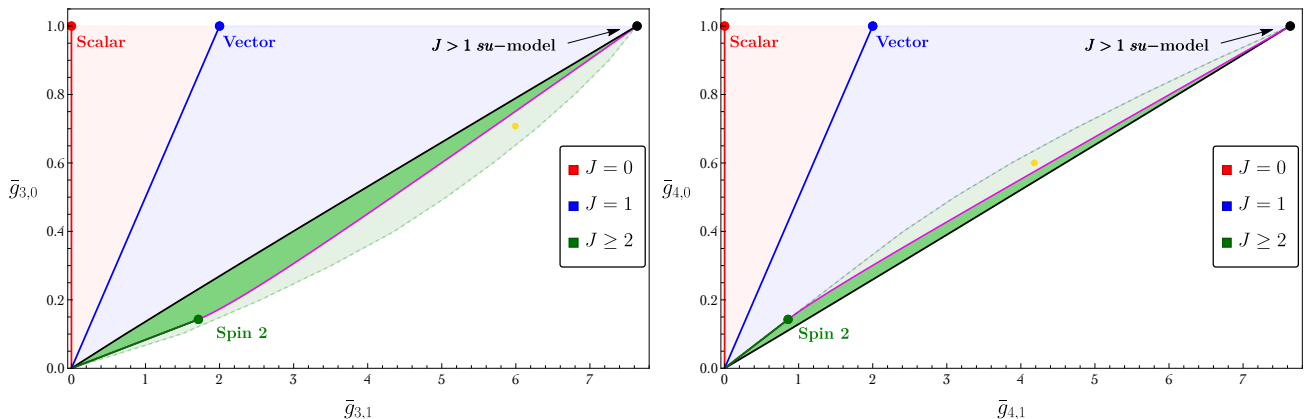


Figure 7: Allowed region in the $\bar{g}_{3,1}$ – $\bar{g}_{3,0}$ plane (left) and $\bar{g}_{4,1}$ – $\bar{g}_{4,0}$ plane (right) from positivity. The black lines correspond to the $J > 1$ su -model (Eq. (97) with Eq. (98) and $0 \leq m \leq M$), the green lines to $J = 2$ models, and the magenta lines to Eq. (69) and Eq. (70) for the left and right plot respectively. The green areas limited by the dashed line corresponds to the allowed region with $n_{\max} = 7$ null constraints.

At order $O(s^3)$ and $O(s^4)$ we can also consider $(\bar{g}_{3,1}, \bar{g}_{3,0})$ and $(\bar{g}_{4,1}, \bar{g}_{4,0})$. The contributions from models of scalars and vectors are given by the lines going respectively from the points $(0, 1)$ and $(2, 1)$ to the origin, illustrated in Fig. 7 in red and blue.

The allowed regions for $J \geq 2$ are less trivial, and correspond to the green areas in Fig. 7. Again the upper kink is associated with the su -model, with its degenerate spectrum that makes $\bar{g}_{n,0}$ maximal. The coefficients are

$$(\bar{g}_{n,1}, \bar{g}_{n,0})_{J>1 \text{ } su\text{-model}} = (\approx 7.6, 1), \quad (66)$$

as illustrated by the black dots in Fig. 7. For $m \in [0, M]$, the su -model spans the minimum and maximum of the $J \geq 2$ region of $(\bar{g}_{3,1}, \bar{g}_{3,0})$ and $(\bar{g}_{4,1}, \bar{g}_{4,0})$ respectively (black lines in the figures).

From Eq. (57) the minimal values for $\bar{g}_{n,1}/\bar{g}_{n,0}$ correspond to models with the lowest possible spin. This would mean a theory with $J = 2$ mesons only, but we have seen that this is incompatible with the Froissart-Martin bound: $J \geq 2$ states are also needed to satisfy the null constraints. Although these states can be made infinitely heavy (see section 2.3.3), they only decouple in $\bar{g}_{n,1}$ for $n \geq 4$. Therefore the $J = 2$ theory would give the minimal value for $\bar{g}_{4,1}/\bar{g}_{4,0} = J(J+1)|_{J=2} = 6$, but not for $\bar{g}_{3,1}/\bar{g}_{3,0}$. The amplitude of a single spin-2 meson gives from Eq. (27),

$$(\bar{g}_{4,1}, \bar{g}_{4,0})_{\text{spin-2}} = (6/7, 1/7). \quad (67)$$

Following a similar analysis as in Appendix B, we expect this to be also a kink in the limit where all null constraints are taken into account. The boundary between this kink Eq. (67) and the $J > 1$ su -model has been obtained numerically and is illustrated by the green dashed line in Fig. 7.

For $(\bar{g}_{3,1}, \bar{g}_{3,0})$, we cannot assure the existence of a kink at the $J = 2$ value $(12/7, 1/7)$, but the numerical bound (green dashed line) seems to approach this point.

A consistent amplitude that interpolates between the $J > 1$ su -model and the spin-2 model is given by

$$\widehat{\mathcal{M}} = \mathcal{M}_2^{(su)} - \frac{5(13 \ln 2 - 9)}{g_{f_2 \pi \pi}^2} \left(\widehat{\mathcal{M}}^{(f_2)}(m_{f_2} \rightarrow m) - \widehat{\mathcal{M}}^{(f_2)} \right), \quad (68)$$

and corresponds to the $J > 1$ su -model with the spin-2 state of mass m removed and added back at mass m_{f_2} . In the limit $m_\infty \rightarrow \infty$, Eq. (68) leads to

$$\bar{g}_{3,0} = \frac{20 - 23r^3 + a(-65 + 75r^3)}{140 - 143r^2 + 5a(-91 + 93r^2)}, \quad \bar{g}_{3,1} = \frac{240 - 245r^3 + a(-780 + 798r^3)}{140 - 143r^2 + 5a(-91 + 93r^2)}, \quad (69)$$

$$\bar{g}_{4,0} = \frac{20 - 23r^4 + a(-65 + 75r^4)}{140 - 143r^2 + 5a(-91 + 93r^2)}, \quad \bar{g}_{4,1} = \frac{120 - 125r^4 + 6a(-65 + 68r^4)}{140 - 143r^2 + 5a(-91 + 93r^2)}. \quad (70)$$

where $r = m_{f_2}^2/m^2$ and $a = 1 - \ln 2$, shown in Fig. 7 as magenta lines, and compared to the predictions from the Lovelace-Shapiro amplitude (yellow dot), that lies – again – outside of the area limited by the magenta lines.

4.2 VMD and Spin-2 dominance

As we have seen, for amplitudes satisfying $\mathcal{M}/s^2 \rightarrow 0$ at large energies, spin-1 states decouple and our previous arguments for VMD no longer hold. In this case, spin-1, spin-0 and higher spin contributions are independent phenomenological quantities and VMD would be a mere accident of Nature. In spite of this, we still expect the f_2 coupling to pions to be larger than that for $J \geq 3$ states, in analogy to VMD. To quantify this statement, we define

$$\bar{g}_i^2 = \frac{g_{i\pi\pi}^2}{g_{2,0} m_i^4}, \quad (71)$$

and look for their largest allowed values compatible with positivity. For scalars and vectors, that decouple from the null constraints, we have

$$\bar{g}_s^2, \bar{g}_\rho^2 \leq 1. \quad (72)$$

For the spin-2 state, instead, we obtain

$$\bar{g}_{f_2}^2 \lesssim 0.80. \quad (73)$$

Similarly to the spin-1 meson in the case $\mathcal{M}/s^2 \rightarrow 0$, this latter bound is saturated by the $J > 1$ su -model. The QCD experimental value (extracted from data in [44]) is $\bar{g}_{f_2}^2 = 0.41 \pm 0.25$ and is much smaller than Eq. (73). This is due to the presence of the ρ -meson that also contributes to the normalization factor $g_{2,0}$ and therefore makes $\bar{g}_{f_2}^2$ smaller. For higher-spin states, we find, taking $m_i/m_{f_2} \sim 1.3$,

$$\bar{g}_{\rho_3}^2 \lesssim 0.14, \quad \bar{g}_{f_4}^2 \lesssim 0.04. \quad (74)$$

Interestingly, if we assume $\bar{g}_\rho \neq 0$ (which is not implied by the null constraints), we can still find a bound on the maximal contribution to the Wilson coefficients arising from $J > 1$ states:

$$\frac{\bar{g}_{2,1}}{\bar{g}_{2,1}|_\rho} \lesssim 1 + 0.17 \frac{1 - \bar{g}_\rho^2}{\bar{g}_\rho^2}. \quad (75)$$

Here we have used that theories containing $J \geq 2$ mesons have $\langle 1/m^4 \rangle_{J\text{-odd}} / \langle 1/m^4 \rangle \lesssim 0.17$, with the bound saturated by the $J > 1$ su -model. Taking for instance $\bar{g}_\rho^2 \sim 0.5$, we obtain from Eq. (75) that the ρ contributes $\gtrsim 80\%$: it still dominates, in line with VMD.

5 Conclusions

We have studied pion scattering amplitudes in the large- N_c limit, using dispersion relations based on crossing-symmetry, unitarity and causality of the QCD dynamics. Under different assumptions about the high-energy behavior of amplitudes, but agnostic of the specific meson spectral density, we have identified the allowed regions of parameter space for the low-energy Wilson coefficients.

For amplitudes with $\mathcal{M}(s) \lesssim s$ at high-energy, building upon Ref. [19], we have made progress in several directions. By separating theories with $J = 0$ mesons only, from theories with $J \geq 1$, we have revealed a pattern of kinks that characterizes both the leading and the more irrelevant Wilson coefficients. Some kinks are populated by known theories, such as the linear sigma model (involving only a spin-0 meson in the UV completion) and the (scalarless) su -model, that involves a degenerate spectrum of infinitely many higher-spin resonances. The other kinks appear to be associated with a more complex high-energy spectrum, but a numerical exploration of the constraints converges slowly. In these points, we have been able to solve the null constraints analytically, by translating them into a 1D moment problem, and shown that at the kink sits a theory with a single light spin-1 resonance, the ρ meson.

There is one part of the boundary of the allowed region of Wilson coefficients that still eludes analytic methods: here we have found that the scalar-subtracted Lovelace-Shapiro (and part of the Coon) amplitude, provides the best analytical approximation of the constraints – within the numerical bounds but outside the region spanned by simpler theories. This suggests that possibly another deformation of the Lovelace-Shapiro amplitude exists which better approximates the entire boundary.

We have also shown how the soft high-energy behavior of amplitudes implies, via positivity bounds, Vector Meson Dominance and explains the success of holographic QCD. The reason is that although these models do not incorporate higher-spin states, positivity constraints tell us that their contributions in low-energy quantities have to be small.

For amplitudes that are not as soft at high-energy, but that still respect the Froissart-Martin bound $\mathcal{M}(s) \lesssim s \log^2 s$, we have found that analogous results hold. Now, theories with states with $J = 0$ or $J = 1$ decouple from the rest and can be studied in isolation. The remaining theories with $J \geq 2$ also have kinks, populated by the (scalarless and vectorless) su -model or by a theory with a single light spin-2 meson. In this context, we have highlighted a version of “spin-2 meson dominance”.

The comparison between our results and large- N_c lattice simulations (see Fig. 4) emphasizes the complementarity between the two methods and lies down an exciting symbiotic program that combines analytic and lattice methods to corner QCD.

The physics captured by the chiral Lagrangian is rich and describes many processes beyond $\pi\pi$ scattering: the program of cornering large- N_c QCD with positivity bounds can move forward

in many directions. An important direction for further study would be processes involving pions interacting with external sources, scalars or photons. Here we expect that including full unitarity of the QCD amplitude, as done by Ref. [45] in the context of the a -anomaly, would reveal an interesting interplay between the chiral anomaly, the QED minimal coupling, and the parameters studied in this article. This direction of research is interesting also in the framework of physics beyond the Standard Model, in particular for the question of whether the Higgs is composite or not. There, Ref. [46] proposed a set of power-counting rules (one of which was dubbed *minimal coupling*) which are realized at weak coupling and in string theory – it would be interesting to prove this in the wider context of dispersion relations.

On a different front, it would be interesting to incorporate more systematically real-world QCD data to shape the meson spectrum, or vice-versa, see e.g. [47]. To this goal, it is essential to first understand finite N_c effects, as discussed in the single-flavor case in Refs. [4, 48] – a task that we will leave for future work [49, 50].

From a more technical point of view, it is important to bring the analytic methods we have used in this work into a more systematic tool to identify all theories at the boundary, e.g. via a clever use of Lagrange multipliers and resummations at all orders. This would allow us to understand if the Lovelace-Shapiro amplitude (with subtracted scalars, or scalars and vectors) is indeed extremal or not. Here it would be useful to further understand which deformations of known amplitudes are consistent with unitarity, along the lines of [51–53].

Acknowledgments

F.R. thanks Jan Albert, Adam Falkowski, Felipe Figueroa, Davide Lombardo, Marcos Marino, Leonardo Rastelli, Antonio Rodriguez, Jullian Sonner, Matteo Tacchi and Piotr Tourkine for important discussions. F.S. thanks Filippo Nardi for useful conversations. F.S. and F.R. acknowledge the support of the European Consortium for Astroparticle Theory in the form of an Exchange Travel Grant. We are grateful to the Mainz Institute for Theoretical Physics (MITP) of the Cluster of Excellence PRISMA+ (Project ID 39083149), for its hospitality and support during the workshop *Amplitudes meet BSM*. C.F. is supported by the fellowship FPU18/04733 from the Spanish Ministry of Science, Innovation and Universities. A.P. has been supported by the Catalan ICREA Academia Program, and the grants 2014-SGR-1450, PID2020-115845GB-I00/AEI/10.13039/501100011033. The work of F.R. is supported by the Swiss National Science Foundation under grants no. 200021-205016 and PP00P2-206149.

A Numerical Bootstrap

In this appendix, we briefly explain the numerical optimization procedure used in this article, following [6, 7, 19]. From Eq. (17) we know that,

$$\langle \mathcal{X}_{n,l}(m^2, J) \rangle = 0, \quad \langle \mathcal{Y}_{n,l}(m^2, J) \rangle = 0, \quad (76)$$

while Eq. (12) implies,

$$g_{n+l,l} = \langle g_{n+l,l}(m^2, J) \rangle, \quad \text{where} \quad g_{n+l,l}(m^2, J) = \frac{2^l P_J^{(l)}(1)}{l! m^{2(n+l)}}. \quad (77)$$

If we define the vectors

$$\vec{v}_1 = \begin{pmatrix} 1 \\ 0 \\ \vdots \\ 0 \end{pmatrix}, \quad \vec{v}_n = \begin{pmatrix} 0 \\ 1 \\ \vdots \\ 0 \end{pmatrix}, \quad \vec{v}_{\text{HE}}(m^2, J) = \begin{pmatrix} -g_{1,0}(m^2, J)M^2 \\ -g_{n,l}(m^2, J)M^{2n} \\ \mathcal{Y}_{2,1}(m^2, J) \\ \vdots \end{pmatrix}, \quad (78)$$

then the following equation holds

$$g_{1,0}M^2\vec{v}_1 + g_{n,l}M^{2n}\vec{v}_n + \langle \vec{v}_{\text{HE}}(m^2, J) \rangle = 0. \quad (79)$$

This equation can be adjusted to include more Wilson coefficients. Now, multiplying everything by a vector $\vec{\alpha}$ we can solve the following optimization problem:

$$\begin{aligned} & \text{maximize} && \vec{\alpha} \cdot \vec{v}_1 \\ & \text{such that} && \vec{\alpha} \cdot \vec{v}_{\text{HE}}(m^2, J) \geq 0 \\ & && \vec{\alpha} \cdot \vec{v}_n = \pm 1, \end{aligned} \quad (80)$$

where positivity of the high-energy average and the normalization $\vec{\alpha} \cdot \vec{v}_n = +1$ will yield the upper bound $\tilde{g}_{n,l} \leq -\vec{\alpha}_{(+)} \cdot \vec{v}_1$, while $\vec{\alpha} \cdot \vec{v}_n = -1$ the lower bound $\tilde{g}_{n,l} \geq \vec{\alpha}_{(-)} \cdot \vec{v}_1$.

A problem of this kind is solved using a semidefinite problem solver such as SDPB [54]. Notice that in this procedure, we divided everything by the positive term $g_{1,0}M^2$ and for the last term in Eq. (79) we reabsorbed it in the definition of the high-energy average. Furthermore SDPB can only impose the positivity condition in Eq. (81) at the level of polynomials, therefore we must perform the change of variables $m^2 \rightarrow M^2(1+x)$ with $x \geq 0$ and absorb the common denominator once again in the definition of the high-energy average. We can also implement a mass gap simply by modifying the above change of variables to the one $m^2 \rightarrow M'^2(1+x)$, where M'/M is the mass gap. Numerically, Eq. (79) is evaluated on a grid in x and J . The choice of the maximum value J_{max} depends on the number of null constraints we want to consider; as more null constraints are included, a bigger J_{max} must be chosen in order to ensure the convergence of the bounds.

In the specific case of constraining $\tilde{g}_{2,0}, \tilde{g}_{2,1}$, we input fixed values of $\tilde{g}_{2,0}$, and use

$$\vec{v}_1 + \tilde{g}_{2,0}\vec{v}_2 + \langle \vec{v}_{\text{HE}}(m^2, J) \rangle = 0. \quad (81)$$

Then we probe the allowed values of $\tilde{g}_{2,0}$ to find bounds on $\tilde{g}_{2,1}$,

$$(1 + \tilde{g}_{2,0})\vec{v}_1 + \tilde{g}_{2,1}\vec{v}_2 + \langle \vec{v}_{\text{HE}}(m^2, J) \rangle = 0. \quad (82)$$

To extract a ρ state from the high-energy average and impose a mass gap between the ρ and the spectrum in the UV (as explained in the paragraph above), we define $\vec{v}_\rho = \vec{v}_{\text{HE}}(m_\rho^2, 1)$. Then we start by bounding $\tilde{g}_{2,0}$ via,

$$\vec{v}_1 + \tilde{g}_\rho^2 \vec{v}_\rho + \tilde{g}_{2,0} \vec{v}_2 + \langle \vec{v}_{\text{HE}}(m^2, J)' \rangle = 0. \quad (83)$$

We can both reabsorb the term $\tilde{g}_\rho^2 \vec{v}_\rho$ in \vec{v}_1 if we want to assume a value for the coupling, otherwise we can add it to the high-energy average in the positivity condition Eq. (81). Then we use the allowed values of $\tilde{g}_{2,0}$ to bound $\tilde{g}_{2,1}$ with the equation

$$(1 + \tilde{g}_{2,0}) \vec{v}_1 + \tilde{g}_\rho^2 \vec{v}_\rho + \tilde{g}_{2,1} \vec{v}_2 + \langle \vec{v}_{\text{HE}}(m^2, J)' \rangle = 0. \quad (84)$$

The procedure described above gives the plots shown in Figs. 3,4. As we vary n_{max} (the number of null constraints included), features of the exclusion plots vary.

B Minimum of μ_0

A measure that reproduces Eq. (41) is $d\tilde{\mu}(x) \equiv 4K_0(2\sqrt{x})dx$, where K_0 is the Bessel function of the second kind. The (Stieltjes) moment problem associated with Eq. (42) is indeterminate, in the sense that there exist multiple measures $d\mu(x)$ that give rise to this sequence of moments. For instance, asymptotically $K_0(\sqrt{x}) \rightarrow e^{-\sqrt{x}}$ has the same moments as $e^{-\sqrt{x}}(1 + w \cos \sqrt{x})$ for any w . For this reason, as far as μ_0 is concerned, we will treat the measure as unknown, and employ $d\tilde{\mu}(x)$ only for μ_n , $n \geq 1$.

We separate the integration domain $I \equiv [0, \infty[$ into the origin 0 and $I_L \equiv]0, L]$, where eventually we will take $L \rightarrow \infty$. Physically this corresponds to separate out the contribution of states with infinite mass but fixed spin $J \geq 1$. As noted already on page 12, heavy states contribute more to lower, rather than higher, moments; in what follows we will see that in this case infinitely heavy states ($x = 0$) contribute only to the first moment. Indeed, moments μ_n with $n \geq 1$ have no support on 0 and therefore $\mu_n = \mu_n^{I_L}$, where $\mu_n^{I_L} = \int_{I_L} x^n d\mu(x) > 0$ are also moments. Instead μ_0 has support in 0 (we call it $\mu_0^0 \geq 0$), and we can write $\mu_0 = \mu_0^0 + \mu_0^{I_L} \geq \mu_0^{I_L}$.

To prove that $\mu_0^{I_L}$ can be as small as 1, we define a sequence of functions built using positive powers of x , $f_n(x) = \sum_{k=1}^n a_k x^k$, so that

$$0 \leq 1 - f_n(x) \leq 1 \quad x \in I_L, \quad (85)$$

and such that f_n converges pointwise to unity $\lim_{n \rightarrow \infty} f_n(x) \rightarrow 1$ on I_L (for instance, a candidate for $f_n(x)$ is $1/x$ times the Taylor expansion of $1/x$ in L). Then, integrating over the measure,

$$0 \leq \int_{I_L} (1 - f_n(x)) d\mu(x) = \mu_0^{I_L} - \int_{I_L} f_n(x) d\tilde{\mu}(x), \quad (86)$$

where the last integral can be written in terms of higher moments $\sum_{k=1}^n a_k \mu_k^{I_L}$ and provides an expression for the minimum of $\mu_0^{I_L}$ in terms of higher-moments only. Now we can use the dominated convergence theorem to write

$$\mu_0 \geq \mu_0^L \geq \lim_{n \rightarrow \infty} \int_{I_L} f_n(x) d\tilde{\mu}(x) = \int_{I_L} d\tilde{\mu}(x). \quad (87)$$

Since x corresponds to (the square of) impact parameter, in theories with a mass gap, the measure $\mu(x)$ falls off exponentially at large x .

Since the measure decreases exponentially at large x , the limit $L \rightarrow \infty$ is regular, and the arguments still hold. For $L \rightarrow \infty$, the integral in Eq. (87) is known, and we find, $\mu_0 \geq \int d\tilde{\mu}(x) = 2$ which is equivalent to

$$\tilde{g}_{2,0} \leq \frac{1}{3}. \quad (88)$$

This implies that the kink must lie at $(\tilde{g}_{2,1}, \tilde{g}_{2,0}) = (4/3, 1/3)$, corresponding to a theory of a spin-1 particle at mass M , and higher-spin states at ∞ , as in Eq. (25).

Higher kinks. These arguments can be exploited also to obtain the kink positions in the planes of other Wilson coefficients. In particular, *considering only spins $J \geq 1$* (i.e. singling out the spin-0 contribution), one finds that the allowed regions of $(\tilde{g}_{n,1}, \tilde{g}_{n,0})$ have also kinks, see Fig. 5. Again, numerically the position of such kinks converges very slowly, but analytically we can prove that their position is at,

$$(\tilde{g}_{n,1}, \tilde{g}_{n,0}) = (2/3, 1/3), \quad \text{for } n > 2. \quad (89)$$

Indeed, from Eq. (57), we have for $J \geq 1$ that $\frac{g_{n,1}}{g_{n,0}} \geq 2$. Moving along the extremal line $g_{n,1} = 2g_{n,0}$, corresponding to a spin-1 state, the kink resides at the largest value of $g_{n,0}/g_{1,0}$. To find this value one has to ask whether it is possible add to the spin-1 state a spectrum of states that enhance $g_{n,0}/g_{1,0}$ without affecting the ratio $g_{n,1}/g_{n,0}$ ($n = 3, 4, \dots$). This latter condition implies, from Eq. (57), $\langle \frac{\mathcal{J}^2}{m^{2n}} \rangle \rightarrow 0$ and therefore also $\langle 1/m^{2n} \rangle \rightarrow 0$. This leads to

$$\tilde{g}_{n,0} = \frac{1}{1 + \frac{M^2}{g_{\rho\pi\pi}^2} \langle \frac{1}{m^2} \rangle}. \quad (90)$$

Following the same reasoning as before, one can obtain that $\frac{M^2}{g_{\rho\pi\pi}^2} \langle \frac{1}{m^2} \rangle \geq 2$, and therefore $\tilde{g}_{n,0} \leq 1/3$, leading to Eq. (89). Also this kink lies at the extremum of the spin-1 line.

C The su -models

Let us consider the most general theory of a degenerate spectrum that contributes to the four-pion amplitude $\mathcal{M}(s, u)$ [6, 7]. This means that all states have equal mass m , and therefore the denominator of this amplitude is fixed to be $\mathcal{M}(s, u) \propto 1/((s - m^2)(u - m^2))$. If we further demand that Eq. (6a) and Eq. (6b) are satisfied for $k_{\min} = 1$, we are led to

$$\mathcal{M}(s, u) = \frac{a_1 m^4 + a_2 m^2 (s + u) + a_3 s u}{(s - m^2)(u - m^2)}, \quad (91)$$

where a_i are constants. The Adler's zero condition fixes $a_1 = 0$. Then, aside from a global multiplicative factor, the amplitude has only one free parameter. We can write it as

$$\mathcal{M}_1^{(su)}(s, u) = \frac{m^2 (s + u) + \lambda s u}{(s - m^2)(u - m^2)}, \quad (92)$$

where the possible values of λ are determined by unitarity. Indeed, imposing the positivity of the residues of Eq. (92), we obtain

$$-2 \leq \lambda \leq \frac{2 \ln 2 - 1}{1 - \ln 2}. \quad (93)$$

In the limiting case $\lambda = -2$, the residues of all $J > 0$ states are zero, and we are left with the scalar amplitude Eq. (22). In the other limit,

$$\lambda = \frac{2 \ln 2 - 1}{1 - \ln 2} \simeq 1.26, \quad (94)$$

the residue of the spin-0 state is zero, leading to an amplitude mediated by an infinite tower of states of spin $J > 0$ and mass m . We will refer to this latter case as the $J > 0$ su -model.

Expanding Eq. (92) for $s, u \ll m^2$, we can obtain the Wilson coefficients:

$$g_{n,0} = \frac{1}{m^{2n}}, \quad g_{n,l} = \frac{2 + \lambda}{m^{2n}} \quad (n, l > 0). \quad (95)$$

For Eq. (94), the Wilson coefficients, normalized as in Eq. (30) for $M = m$, are given by

$$\tilde{g}_{n,0} = 1, \quad \tilde{g}_{n,l} = \frac{1}{1 - \ln 2} \simeq 3.26 \quad (n > 1, l > 0). \quad (96)$$

These are shown in Figs. 3–5 as a black dot.

We can proceed in a similar way to construct the most general amplitude of degenerate high-spin states, but now satisfying Eq. (6a) and Eq. (6b) for $k_{\min} = 2$. Imposing the Adler's zero condition, such amplitude is given by (up to a multiplicative constant factor)

$$\mathcal{M}_2^{(su)}(s, u) = \frac{m^2(s + u) + \lambda_1 su + \lambda_2(s^2 + u^2)}{(s - m^2)(u - m^2)}. \quad (97)$$

The values of the constants λ_1 and λ_2 determine different theories according to:

- For $2 + \lambda_1 + 2\lambda_2 = 0$, the residues for $J > 1$ vanish and we have a theory with only a spin-0 and spin-1 state.
- For $\lambda_2 = (2 + \lambda_1) \frac{6 \ln 8 - 12}{25 - 36 \ln 2}$, the residue for the spin-1 state is zero and we have a theory with $J = 0$ and $J > 1$.
- For $\lambda_2 = -1 + \frac{1 - \lambda_1(\ln 4 - 2)}{\ln 16 - 1}$, the residue for the spin-0 vanishes and we have a theory with spins $J > 0$.

Furthermore, for $\lambda_1 = -2$, $\lambda_2 = 0$, we recover the scalar amplitude Eq. (22), while for $\lambda_1 = \lambda_2 = -2/3$ we obtain the spin-1 amplitude Eq. (24). We are interested in the case where the amplitude Eq. (97) contains only $J > 1$ states which corresponds to taking

$$\lambda_1 = \frac{20 \ln 2 - 13}{19 - 28 \ln 2}, \quad \lambda_2 = \frac{6 \ln 8 - 12}{19 - 28 \ln 2}. \quad (98)$$

We will refer to this case as the $J > 1$ su -model.

The Wilson coefficients of Eq. (97) are given by

$$\begin{aligned} g_{1,0} &= \frac{1}{m^2}, & g_{2,1} &= \frac{2 + \lambda_1}{m^4}, & g_{n,0} &= \frac{1 + \lambda_2}{m^{2n}} \quad (n > 1), \\ g_{n,1} &= \frac{2 + \lambda_1 + \lambda_2}{m^{2n}}, & g_{n,l} &= \frac{2 + \lambda_1 + 2\lambda_2}{m^{2n}} \quad (n, l > 1). \end{aligned} \quad (99)$$

For the case Eq. (98), normalizing the coefficients as given in Eq. (63), we have

$$\bar{g}_{n,0} = 1, \quad \bar{g}_{n,1} = \frac{18 \ln 2 - 13}{10 \ln 2 - 7} \simeq 7.64, \quad \bar{g}_{n,l} = \frac{1}{7 - 10 \ln 2} \simeq 14.59 \quad (n > 2, l > 1). \quad (100)$$

These are shown in Fig. 7 as a black dot.

C.1 Two-mass su -model

The su -models define part of the boundaries of the allowed regions of the Wilson coefficients. To see this, we can deform the above su -models by introducing an additional pole in the amplitude, i.e., $\mathcal{M}(s, u) \propto 1/((s - m^2)(u - m^2)(s - M^2)(u - M^2))$. In this case the most general amplitude can be written as

$$\mathcal{M}(s, u) = \mathcal{M}_1^{(su)}(m) + \alpha \mathcal{M}_1^{(su)}(M) + \frac{\beta s^2 u^2}{(s - m^2)(u - m^2)(s - M^2)(u - M^2)}, \quad (101)$$

that corresponds to two su -models (Eq. (92)) with mass m and M respectively, and an extra term. Apart from the masses, the amplitude has 4 parameters: the two λ of the su -models, α and β . We are interested in this model without the scalars. Removing the scalars in the two su -models fixes the λ 's to the value Eq. (94). Removing the scalar from the last term of Eq. (101) corresponds to adding to the amplitude the term

$$\beta \left[f(m, M) \left(\frac{1}{s - m^2} + \frac{1}{u - m^2} \right) + (M \leftrightarrow m) \right], \quad (102)$$

where

$$f(m, M) = \frac{m^4 M^2 + m^6 (\ln 2 - 1) + m^2 M^4 \ln \frac{M^2}{m^2 + M^2}}{(m^2 - M^2)^2}. \quad (103)$$

Requiring the positivity of the spectral function for the $J > 0$ states in Eq. (101) leads to $\beta \geq 0$.

Eq. (101) with Eq. (102) leads to

$$\frac{\tilde{g}_{2,1}}{\tilde{g}_{2,0}} = \frac{3.26 \left(\frac{1}{m^4} + \frac{a}{M^4} \right)}{\left(\frac{1}{m^4} + \frac{a}{M^4} \right) - \beta \left(\frac{f(m, M)}{m^4} + \frac{f(M, m)}{M^4} \right)}. \quad (104)$$

Since $\beta \left(\frac{f(m, M)}{m^4} + \frac{f(M, m)}{M^4} \right)$ is a positive-definite function, we see that the ratio $\tilde{g}_{2,1}/\tilde{g}_{2,0}$ is bounded from below by the su -model.

D The Lovelace-Shapiro amplitude

The Lovelace-Shapiro (LS) amplitude for the scattering of four pions is defined as [20, 21]

$$\mathcal{M}^{(\text{LS})}(s, u) = \frac{\Gamma(1 - \alpha(s))\Gamma(1 - \alpha(u))}{\Gamma(1 - \alpha(s) - \alpha(u))}, \quad (105)$$

where $\alpha(s) = \alpha_0 + \alpha' s$ is referred as the Regge trajectory. We will fix the values of α_0 and α' by requiring that Eq. (106) satisfies the Adler zero condition, $\mathcal{M}^{(\text{LS})}(s, u) \rightarrow 0$ for $s, u \rightarrow 0$, and that the first pole of Eq. (106) occurs for $s = m_\rho^2$. These two conditions lead to $\alpha_0 = 1/2$ and $\alpha' = 1/(2m_\rho^2)$ [55] and then we can write

$$\mathcal{M}^{(\text{LS})}(s, u) = \frac{\Gamma\left(\frac{1}{2} - \frac{s}{2m_\rho^2}\right)\Gamma\left(\frac{1}{2} - \frac{u}{2m_\rho^2}\right)}{\Gamma\left(\frac{t}{2m_\rho^2}\right)}. \quad (106)$$

By looking at the poles of Eq. (106), one can see that the LS amplitude corresponds to a theory of higher-spin states with masses

$$m_n^2 = m_\rho^2(2n + 1), \quad n = 0, 1, 2, \dots \quad (107)$$

For a given n , there are at most $n + 1$ states with spin $J = 0, 1, \dots, n + 1$. Furthermore, Eq. (106) satisfies the condition Eq. (6a) and Eq. (6b) with $k_{\min} = 1$.

The first Wilson coefficients arising from Eq. (106) in a low-energy expansion are given by

$$g_{1,0} = \frac{\pi}{2m_\rho^2}, \quad g_{2,0} = \frac{1}{2}g_{2,1} = \frac{\pi \ln 2}{2m_\rho^4}, \quad g_{3,0} = \frac{\pi^3 + 12\pi \ln^2 2}{48m_\rho^6}, \quad (108)$$

$$g_{3,1} = \frac{3\pi \ln^2 2}{4m_\rho^6}, \quad g_{4,0} = \frac{\pi(\pi^2 \ln 2 + 4 \ln^3 2 + 6\zeta(3))}{48m_\rho^8}, \quad (109)$$

$$g_{4,1} = \frac{\pi(\pi^2 \ln 2 + 16 \ln^3 2 + 3\zeta(3))}{48m_\rho^8}, \quad g_{4,2} = \frac{\pi(4 \ln^3 2 - \zeta(3))}{8m_\rho^8}, \quad (110)$$

with ζ the Riemann zeta function. For the normalized Wilson coefficients defined in Eq. (30) we have, taking $M = m_\rho$,

$$\tilde{g}_{2,0} \simeq 0.69, \quad \tilde{g}_{2,1} \simeq 1.39, \quad \tilde{g}_{3,0} \simeq 0.65, \quad \tilde{g}_{3,1} \simeq 0.72, \quad \tilde{g}_{4,0} \simeq 0.64, \quad \tilde{g}_{4,1} \simeq 0.66, \quad \tilde{g}_{4,2} \simeq 0.03, \quad (111)$$

while for the normalized coefficients in Eq. (63), we have

$$\bar{g}_{2,1} \simeq 2, \quad \bar{g}_{3,0} \simeq 0.94, \quad \bar{g}_{3,1} \simeq 1.04, \quad \bar{g}_{4,0} \simeq 0.92, \quad \bar{g}_{4,1} \simeq 0.95, \quad \bar{g}_{4,2} \simeq 0.05. \quad (112)$$

Since a theory of scalars provides a consistent UV completion of the pion amplitude \mathcal{M} , satisfying Eq. (6a) and Eq. (6b) with $k_{\min} = 1$, we can find a new consistent amplitude by subtracting the scalars from Eq. (106). This leads to

$$\mathcal{M}_{J>0}^{(\text{LS})}(s, u) = \mathcal{M}^{(\text{LS})}(s, u) - \sum_{n=0}^{\infty} \left[\frac{m_n^2}{s - m_n^2} \kappa_{s,0}^{\text{LS}} + (s \leftrightarrow u) \right], \quad (113)$$

with

$$\kappa_{s,J}^{\text{LS}} = \frac{2J+1}{2} \int_{-1}^1 dx P_J(x) \text{Res}_{s=m_n^2} [\mathcal{M}^{(\text{LS})}(s, u(x))] , \quad (114)$$

where $u(x) = -s(1-x)/2$. From Eq. (113), we obtain by expanding at small s, u :

$$\tilde{g}_{2,0} \simeq 0.55, \quad \tilde{g}_{2,1} \simeq 2.05, \quad \tilde{g}_{3,0} \simeq 0.49, \quad \tilde{g}_{3,1} \simeq 1.07, \quad \tilde{g}_{4,0} \simeq 0.48, \quad \tilde{g}_{4,1} \simeq 0.97, \quad \tilde{g}_{4,2} \simeq 0.05. \quad (115)$$

In a similar way, we can also remove the (infinite) spin-1 states of Eq. (113) to obtain an amplitude that still satisfies the Froissart-Martin condition, Eq. (6a) and Eq. (6b) with $k_{\min} = 2$:

$$\mathcal{M}_{J>1}^{(\text{LS})}(s, u) = \mathcal{M}_{J>0}^{(\text{LS})}(s, u) - \sum_{n=0}^{\infty} \left[\frac{m_n^2 + 2u}{s - m_n^2} \kappa_{s,1}^{\text{LS}} + (s \leftrightarrow u) \right]. \quad (116)$$

From Eq. (116) we obtain

$$\bar{g}_{2,1} \simeq 0.97, \quad \bar{g}_{3,0} \simeq 0.71, \quad \bar{g}_{3,1} \simeq 5.99, \quad \bar{g}_{4,0} \simeq 0.60, \quad \bar{g}_{4,1} \simeq 4.18, \quad \bar{g}_{4,2} \simeq 8.15. \quad (117)$$

E The Coon amplitude

The Lovelace-Shapiro amplitude presented in Appendix D can be generalized to a larger class of amplitudes depending on an additional parameter q . This is the so-called Coon amplitude, which was first proposed in [22]⁹:

$$\mathcal{M}_q(s, u) = C(\sigma, \tau, q) \prod_{n=0}^{\infty} \frac{(1 - q^{n+1})(\sigma\tau - q^{n+1})}{(\sigma - q^{n+1})(\tau - q^{n+1})}, \quad (118)$$

where $\sigma = 1 + (q-1)(\alpha_0 + \alpha's)$ and $\tau = 1 + (q-1)(\alpha_0 + \alpha'u)$. As explained in Appendix D, we take $\alpha_0 = 1/2$ and $\alpha' = 1/(2m_\rho^2)$. The parameter q takes values between 0 and 1, and in the limit $q \rightarrow 1$ we recover the LS amplitude Eq. (106). There is some freedom in the choice of the prefactor C , as long as it satisfies $\lim_{q \rightarrow 1} C(\sigma, \tau, q) = 1$.

The Coon amplitude has an infinite number of simple poles at

$$s_n = m_\rho^2 \frac{1+q-2q^{n+1}}{1-q}, \quad n = 0, 1, 2, \dots \quad (119)$$

The corresponding residues are

$$\text{Res}_{s=s_n} \mathcal{M}_q(s, u) = C(\sigma_n, \tau, q) \frac{2q^{n+1}}{1-q} \frac{\tau-1}{\tau^{n+1}} m_\rho^2 \prod_{l=0}^{n-1} \frac{(\tau - q^{l-n})}{(1 - q^{l-n})}, \quad (120)$$

⁹The idea of the Coon amplitude goes back to an earlier work by Coon [56], where he defined a generalization of the Veneziano amplitude which was slightly different from Eq. (118). Shortly after that he proposed the Coon version of Lovelace-Shapiro amplitude together with Sukhatme and Tran Thanh Van in [22].

where $\sigma_n = \sigma(s = s_n)$. It is important to remark that the spectrum has an *accumulation point* at $s_* = \lim_{n \rightarrow \infty} s_n = m_\rho^2 \frac{1+q}{1-q}$. In the limit $q \rightarrow 1$, the accumulation point is located at infinity and we recover the evenly-spaced spectrum of the LS amplitude.

It is customary to fix the prefactor $C(\sigma, \tau, q)$ with the further assumption that the residues of the Coon amplitude are polynomials in u , since it is believed that non-polynomial residues lead to problems with the locality of the theory. The prefactor is in this case set to

$$C(\sigma, \tau, q) = q^{\frac{\ln \sigma \ln \tau}{\ln q \ln q}}, \quad (121)$$

which reduces to $C(\sigma_n, \tau, q) = \tau^{n+1}$ at the s_n pole. This term cancels the factor τ^{n+1} in the denominator of Eq. (120) and ensures that the residues are polynomials. In this case, we have that for any n , there are $n + 1$ states with spin $J = 0, 1, \dots, n + 1$, as in the LS amplitude.

Using the prefactor Eq. (121) makes however the Coon amplitude Eq. (118) non-meromorphic. In addition to the simple poles, there is a branch cut starting at the accumulation point s_* . Although the physical meaning of this kind of singularities is unclear, amplitudes with branch cuts can still obey the requirements of unitarity, crossing symmetry and Regge boundedness, so it is interesting to include them in our study.

Regarding the high-energy behavior, the amplitude with prefactor Eq. (121) grows at fixed u like $\mathcal{M}_q(s, u) \sim f(u) s^{\ln \tau / \ln q}$. For negative u , $\ln \tau / \ln q < 0.5$, so the amplitude obeys Eq. (6a) for $k_{\min} = 1$. At fixed t , the amplitude grows like $\mathcal{M}_q(s, u) \sim s^{\ln((1-q)\alpha' s) / \ln q}$. Since $\ln((1-q)\alpha' s) / \ln q < 0.5$, it also obeys Eq. (6b) for $k_{\min} = 1$.

The last point to address is the unitarity of the Coon amplitude. We have found that the $J = 0$ states have negative residues for all $n > 0$, making the amplitude non-unitary. This result is in agreement with the early study [57]¹⁰, which pointed out the presence of ghosts. On the other hand, we have found that the rest of the J states have positive residues inside the scope of our numerical searches. As for the branch cut discontinuity, it can also be expanded in partial waves according to Eq. (8). We have obtained that the spectral density $\rho_J(s)$ is positive for all J except from $J = 0$. Due to this problems, we will not discuss this case further.

On the other hand, relaxing the assumption of polynomial residues, we can simply take $C(\sigma, \tau, q) = 1$, and the amplitude becomes meromorphic (there is no branch cut). We now have an infinite number of spins present for each n . At large s , taking both fixed u and t , we have $\mathcal{M}_q(s, u) \sim \text{constant}$. Therefore it satisfies both Eq. (6a) and Eq. (6b) for $k_{\min} = 1$. For $C(\sigma, \tau, q) = 1$ we have also found that the only negative residue corresponds to the $J = 0$, $n = 1$ state only in the small region $0.94 \lesssim q < 1$.

The contribution of the Coon amplitude with $C = 1$ is shown in Fig. 3 for $q \in [0, 1]$. We also show the case in which all scalars are removed from the spectrum. In the limit $q \rightarrow 1$ the Coon amplitude approaches the $J > 0$ Lovelace-Shapiro model, while for $q \rightarrow 1$, the Coon amplitude is dominated by the $n = 0$ level (the $n > 0$ levels decouple), giving the $J > 0$ su -model.

¹⁰Some recent works [58–60] on the Veneziano version of the Coon amplitude have shown that it is unitary in $D = 4$ dimensions. Our result agrees with the results of Coon and Yu [57], who considered the Lovelace-Shapiro version of the Coon amplitude.

References

- [1] A. Adams, N. Arkani-Hamed, S. Dubovsky, A. Nicolis, and R. Rattazzi, *JHEP* **10**, 014 (2006), arXiv: [hep-th/0602178](#).
- [2] N. Arkani-Hamed, T.-C. Huang, and Y.-T. Huang, *JHEP* **05**, 259 (2021), arXiv: [2012.15849](#).
- [3] C. de Rham, S. Melville, A. J. Tolley, and S.-Y. Zhou, *Phys. Rev.* **D96**, 081702 (2017), arXiv: [1702.06134](#).
- [4] B. Bellazzini, J. Elias Miró, R. Rattazzi, M. Riembau, and F. Riva, *Phys. Rev. D* **104**, 036006 (2021), arXiv: [2011.00037](#).
- [5] A. J. Tolley, Z.-Y. Wang, and S.-Y. Zhou (2020), arXiv: [2011.02400](#).
- [6] S. Caron-Huot and V. Van Duong, *JHEP* **05**, 280 (2021), arXiv: [2011.02957](#).
- [7] S. Caron-Huot, D. Mazac, L. Rastelli, and D. Simmons-Duffin (2021), arXiv: [2102.08951](#).
- [8] T. N. Pham and T. N. Truong, *Phys. Rev.* **D31**, 3027 (1985).
- [9] B. Ananthanarayan, D. Toublan, and G. Wanders, *Phys. Rev. D* **51**, 1093 (1995), arXiv: [hep-ph/9410302](#).
- [10] M. R. Pennington and J. Portoles, *Phys. Lett. B* **344**, 399 (1995), arXiv: [hep-ph/9409426](#).
- [11] J. Bijnens, G. Colangelo, G. Ecker, J. Gasser, and M. E. Sainio, *Nucl. Phys. B* **508**, 263 (1997), [Erratum: *Nucl.Phys.B* 517, 639–639 (1998)], arXiv: [hep-ph/9707291](#).
- [12] B. Ananthanarayan, G. Colangelo, J. Gasser, and H. Leutwyler, *Phys. Rept.* **353**, 207 (2001), arXiv: [hep-ph/0005297](#).
- [13] G. Colangelo, J. Gasser, and H. Leutwyler, *Nucl. Phys. B* **603**, 125 (2001), arXiv: [hep-ph/0103088](#).
- [14] A. V. Manohar and V. Mateu, *Phys. Rev. D* **77**, 094019 (2008), arXiv: [0801.3222](#).
- [15] A. L. Guerrieri, J. Penedones, and P. Vieira, *Phys. Rev. Lett.* **122**, 241604 (2019), arXiv: [1810.12849](#).
- [16] A. Guerrieri, J. Penedones, and P. Vieira (2020), arXiv: [2011.02802](#).
- [17] G. 't Hooft, *Nucl. Phys. B* **72**, 461 (1974).
- [18] E. Witten, *Nucl. Phys. B* **160**, 57 (1979).
- [19] J. Albert and L. Rastelli, *JHEP* **08**, 151 (2022), arXiv: [2203.11950](#).
- [20] C. Lovelace, *Phys. Lett. B* **28**, 264 (1968).

- [21] J. A. Shapiro, Phys. Rev. **179**, 1345 (1969).
- [22] D. D. Coon, U. P. Sukhatme, and J. Tran Thanh Van, Phys. Lett. B **45**, 287 (1973).
- [23] J. J. Sakurai, *Currents and mesons* (Chicago U. P., 1969).
- [24] G. Ecker, J. Gasser, A. Pich, and E. de Rafael, Nucl. Phys. B **321**, 311 (1989).
- [25] J. Erlich, E. Katz, D. T. Son, and M. A. Stephanov, Phys. Rev. Lett. **95**, 261602 (2005), arXiv: hep-ph/0501128.
- [26] L. Da Rold and A. Pomarol, Nucl. Phys. B **721**, 79 (2005), arXiv: hep-ph/0501218.
- [27] M. Froissart, Phys. Rev. **123**, 1053 (1961).
- [28] A. Martin, Phys. Rev. **129**, 1432 (1963).
- [29] Y. S. Jin and A. Martin, Phys. Rev. **135**, B1375 (1964).
- [30] K. Häring and A. Zhiboedov (2022), arXiv: 2202.08280.
- [31] M. Herrero-Valea, R. Santos-Garcia, and A. Tokareva, Phys. Rev. D **104**, 085022 (2021), arXiv: 2011.11652.
- [32] B. Bellazzini, F. Riva, J. Serra, and F. Sgarlata, JHEP **10**, 189 (2019), arXiv: 1903.08664.
- [33] S. El-Showk, M. F. Paulos, D. Poland, S. Rychkov, D. Simmons-Duffin, and A. Vichi, Phys. Rev. D **86**, 025022 (2012), arXiv: 1203.6064.
- [34] J. Lasserre, Imperial College Press (2009).
- [35] E. L. Basor, Y. Chen, and H. Widom, Journal of Functional Analysis **179**, 214 (2001), ISSN 0022-1236, URL <https://www.sciencedirect.com/science/article/pii/S0022123600936723>.
- [36] D. Toublan and J. J. M. Verbaarschot, Nucl. Phys. B **603**, 343 (2001), arXiv: hep-th/0012144.
- [37] G. Akemann (2016), arXiv: 1603.06011.
- [38] J. Bijnens, G. Colangelo, and J. Gasser, Nucl. Phys. B **427**, 427 (1994), arXiv: hep-ph/9403390.
- [39] G. S. Bali, F. Bursa, L. Castagnini, S. Collins, L. Del Debbio, B. Lucini, and M. Panero, JHEP **06**, 071 (2013), arXiv: 1304.4437.
- [40] P. Hernández, C. Pena, and F. Romero-López, Eur. Phys. J. C **79**, 865 (2019), arXiv: 1907.11511.

- [41] J. Baeza-Ballesteros, P. Hernández, and F. Romero-López, *JHEP* **06**, 049 (2022), arXiv: 2202.02291.
- [42] J. Gasser and H. Leutwyler, *Nucl. Phys. B* **250**, 465 (1985).
- [43] G. Panico and A. Wulzer, *JHEP* **05**, 060 (2007), arXiv: hep-th/0703287.
- [44] R. L. Workman et al. (Particle Data Group), *PTEP* **2022**, 083C01 (2022).
- [45] D. Karateev, J. Marucha, J. a. Penedones, and B. Sahoo (2022), arXiv: 2204.01786.
- [46] G. F. Giudice, C. Grojean, A. Pomarol, and R. Rattazzi, *JHEP* **06**, 045 (2007), arXiv: hep-ph/0703164.
- [47] I. Caprini, G. Colangelo, and H. Leutwyler, *Eur. Phys. J.* **C72**, 1860 (2012), arXiv: 1111.7160.
- [48] B. Bellazzini, M. Riembau, and F. Riva (2021), arXiv: 2112.12561.
- [49] D. M. Lombardo, Ph.D. thesis, Geneva U., Dept. Theor. Phys. (2022).
- [50] A. Falkowski, D. Lombardo, F. Riva, and A. Rodriguez (In Preparation).
- [51] C. Cheung and G. N. Remmen (2022), arXiv: 2210.12163.
- [52] N. Geiser and L. W. Lindwasser (2022), arXiv: 2210.14920.
- [53] Y.-t. Huang and G. N. Remmen, *Phys. Rev. D* **106**, L021902 (2022), arXiv: 2203.00696.
- [54] D. Simmons-Duffin, *JHEP* **06**, 174 (2015), arXiv: 1502.02033.
- [55] M. Bianchi, D. Consoli, and P. Di Vecchia, *JHEP* **03**, 119 (2021), arXiv: 2002.05419.
- [56] D. D. Coon, *Phys. Lett. B* **29**, 669 (1969).
- [57] D. D. Coon and S. Yu, *Phys. Rev. D* **10**, 3780 (1974).
- [58] F. Figueroa and P. Tourkine, *Phys. Rev. Lett.* **129**, 121602 (2022), arXiv: 2201.12331.
- [59] N. Geiser and L. W. Lindwasser (2022), arXiv: 2207.08855.
- [60] J. Chakravarty, P. Maity, and A. Mishra, *JHEP* **10**, 043 (2022), arXiv: 2208.02735.